AEGIS: AN ADVANCED LATTICE PHYSICS CODE FOR LIGHT WATER REACTOR ANALYSES

AKIO YAMAMOTO[*, 1], TOMOHIRO ENDO[1], MASATO TABUCHI[2], NAOKI SUGIMURA[2], TADASHI USHIO[2], MASAAKI MORI[2], MASAHIRO TATSUMI[3] and YASUNORI OHOKA[3]
[1]Graduate School of Engineering, Nagoya University
Furo-cho, Chikusa-ku, Nagoya, Japan, 464-8603
[2]Nuclear Engineering, Ltd.
[3]Nuclear Fuel Industries, Ltd.
[*]Corresponding author. E-mail : a-yamamoto@nucl.nagoya-u.ac.jp

Received May 31, 2010

AEGIS is a lattice physics code incorporating the latest advances in lattice physics computation, innovative calculation models and efficient numerical algorithms and is mainly used for light water reactor analyses. Though the primary objective of the AEGIS code is the preparation of a cross section set for SCOPE2 that is a three-dimensional pin-by-pin core analysis code, the AEGIS code can handle not only a fuel assembly but also multi-assemblies and a whole core geometry in two-dimensional geometry. The present paper summarizes the major calculation models and part of the verification/validation efforts related to the AEGIS code.

KEYWORDS : AEGIS, Lattice Physics Computation, Resonance Calculation, Method of Characteristics, Burnup Calculation, Verification and Validation

1. INTRODUCTION

In the current light water reactor analysis, the neutronics analysis procedure is divided into two stages – the lattice physics and the core calculations. The former is to make a tabulated cross section set for the latter, commonly on the basis of homogenized fuel assemblies or fuel pincells. The latter performs simulations to obtain the neutronics characteristics of a core. Since the overall performance of a core analysis system is dominated by a weak link in its cascade, the lattice physics and the core analysis codes equally share the responsibility for prediction accuracy.

Improvements in fuel design are continuously performed in order to reduce fuel cycle cost and to increase plant performance. Though such fuel design changes are aimed at improving neutron economy, mechanical behavior and/or thermal hydraulics performance, they may pose challenging situations for a nuclear design code, e.g., when advanced burnable poison containing various burnout speeds, offset water rods of complicated shape and highly heterogeneous fuel such as MOX are involved. In order to handle these issues and to maintain prediction accuracy for neutronics design, continuous efforts are being undertaken by many researchers and engineers.

Development of the AEGIS code is one of these ongoing efforts to improve accuracy and to increase the capability of lattice physics computation.

The AEGIS code is a lattice physics code developed by Nuclear Engineering Ltd. in cooperation with Nagoya University and Nuclear Fuel Industries, Ltd. The primary purpose of the AEGIS code is the preparation of a cross section set for the SCOPE2 code, which is a three-dimensional pin-by-pin core analysis simulator developed by Nuclear Fuel Industries, Ltd. [1]. At this stage of development, goals for the AEGIS code are as follows:

1) Incorporate the latest developments in lattice physics computation.
2) Incorporate calculation models as rigorously as possible, considering practical computation time.
3) Eliminate the conventional "pin-cell" calculation for spatial homogenization and energy condensation in order to reduce uncertainty.
4) Develop and incorporate innovative numerical algorithms for higher calculation efficiency.
5) Enable not only single fuel assembly calculation, but also large scale calculations, such as for a whole core, that can be carried out with a consistent lattice physics computation model.

In Section 2, various calculation models and numerical algorithms to achieve the above objectives are described. Verification and validation results of the calculation models adopted in the AEGIS code are presented in Section 3. Finally, concluding remarks are presented in Section 4.

2. METHODOLOGIES

2.1 Cross Section Library

The AEGIS code has two different cross section libraries: the multi-group cross section library and the ultra-fine group cross section library.

The multi-group cross section library contains cross sections of various nuclides with their dependencies on temperature and background cross section. Though the ultra-fine group cross section library is usually used for the resonance calculation as described later, the AEGIS code can also perform neutronics calculations using only the multi-group cross section library if the equivalence theory is used to prepare effective microscopic cross sections.

The multi-group cross section library is generated through the cross section processing code, NJOY [2]. The multi-group cross section library of the AEGIS code has the following features:

- It is based on the latest nuclear data library, ENDF/B-VII [3]. In addition to ENDF/B-VII, ENDF/B-VI.8 and JENDL3.3 can be used as the alternative cross sections.
- It contains 43 heavy nuclides and 305 other nuclides including 193 fission products so that it can cover the U-Pu burnup chain (i.e., typical U and MOX fuels) and the Th-U burnup chain (Th fuel). Furthermore, various burnable poisons, i.e., B, Cd-In, Eu-Gd, Gd and Er-Tm can be treated.
- The XMAS energy group structure with 172 energy groups is adopted considering the balance between calculation accuracy and computation time [4]. Since the AEGIS code performs assembly transport calculation using the library energy group, a more detailed energy group structure such as the 281 group SHEM would require a considerable longer computation time, though such a detailed energy group structure offers better accuracy.
- Anisotropic scattering cross sections up to the P3 component are stored for light nuclides (e.g., H, O), structural nuclides (e.g., Fe) and major heavy nuclides (e.g., U). This is because the impact of the anisotropic scattering could be significant for MOX fuels in which angular flux distributions show skewed shapes [5]. Furthermore, advanced fuel assemblies appearing in generation-IV reactors have strong heterogeneity; thus, they also require precise treatment of anisotropic scattering. The previous studies on anisotropic scattering suggest that treatment up to the P3 components has sufficient accuracy for highly heterogeneous fuels such as MOX [5].
- Dependence of microscopic cross section on the temperature and the background cross section is considered for all energy ranges, even for scattering matrices. In conventional lattice physics codes such as WIMS, dependence of the microscopic cross section on the background cross section is considered only for the groupwise cross sections (e.g., capture, fission, and total cross sections) in the resonance energy range. Similarly, temperature dependence is treated only for the groupwise cross sections in the resonance energy range. Even though such treatments contribute to the reduction of the size of a cross section library, it may become a source of error. The cross section library of the AEGIS code can avoid such potential inaccuracy.
- The thermal cut-off energy is set to 4.0eV in order to sufficiently cover the upscattering. Since there are several resonances in Pu isotopes, higher thermal cut-off energy is important for accurate prediction, especially for MOX fuel.

The ultra-fine energy group library contains point-wise cross sections of all nuclides treated in the multi-group cross section library (thus, 43 heavy and 305 other nuclides). The ultra-fine group cross section library is used to perform the resonance calculation based on the ultra-fine energy group spectrum method. The major features of this cross section library are summarized as follows:

- All the data are based on ENDF/B-VII
- The energy range from 10MeV to 0.1eV is divided into 32,000 groups. Notably, the energy range below 10keV, which covers the resolved resonance range for major nuclides, is divided into very fine groups. The number of energy groups is chosen from preliminary sensitivity calculations [6].
- Temperature dependence is explicitly considered.

The above two different cross section libraries are both managed with an index-type structure. Similar to the cross section libraries of the continuous energy Monte-Carlo code MCNP [7] or MVP [8], cross sections for a nuclide are stored in an independent file and collections of the cross section files are managed with an index file, in which correspondence between a nuclide name and its actual data file is defined as a list. The AEGIS code accesses the index file first, and then the required microscopic cross section is loaded on an on-demand basis. Since cross sections of different nuclides are stored in independent files, management and maintenance are easy. For example, we can easily change a cross section of a particular nuclide for a sensitivity analysis, which is commonly carried out to investigate the impact of nuclear data on the core (fuel assembly) characteristics.

Cross section library files are generated through the NJOY code [2]. Since the number of processed nuclides is large, a dedicated pre- and post- processing system for the NJOY code is developed and used [9]. The pre-processing code automatically generates an input data file for NJOY from minimal user supplied input data and the execution environment for subsequent calculations of NJOY. After the NJOY calculations, the post-processing code corrects generated cross sections from NJOY in the

MATXSR format, and then performs post editing to generate the final product, i.e., the cross section library for AEGIS.

2.2 Resonance Calculation

2.2.1 Overview

Accuracy of the effective cross section is one of the dominant factors affecting the prediction accuracy of a neutronics evaluation. Evaluation of the effective cross section, i.e., the resonance calculation, is a complicated task and thus various resonance calculation methods have been developed. In this context, the specific resonance calculation method could be a unique feature of a lattice physics code.

In the AEGIS code, two resonance calculation methods are used – the equivalence theory and the ultra-fine group spectrum calculation method. The basic equivalence theory based on Wigner's rational approximation [10] is used for the unresolved energy range since the accuracy of the effective cross section in this energy range is not very important in light water reactor analysis. The resolved resonance energy range, which dominates the accuracy of the lattice physics computation, is treated by the ultra-fine group method [6]. In the following subsections, details of the resonance calculation method focusing on the ultra-fine group method are described.

2.2.2 Ultra-Fine Group Method

The AEGIS code adopts the ultra-fine group spectrum calculation method for the resolved energy range. Its accuracy is very good since the ultra-fine group method directly performs numerical calculation of the slowing down equation in a heterogeneous geometry with actual compositions and then calculates the effective cross section using the resulting detailed energy spectrum. The present method can naturally incorporate the resonance interference effect among different nuclides, which requires a cumbersome treatment in other resonance calculation methods and has considerable impact on calculation accuracy.

The neutron slowing down equation in heterogeneous geometry is given as follows:

$$\Sigma_{t,i}(E)\phi_i(E)V_i=\sum_j P_{j\to i}(E)V_j\left(\begin{array}{l}\int_0^\infty dE'\Sigma_{s,j}(E'\to E)\phi_j(E')\\ +\chi_j(E)\int_0^\infty dE'\nu\Sigma_{f,j}(E')\phi_j(E')\end{array}\right), \quad (1)$$

where

$\sum_{t,i}(E)$ = macroscopic total cross section of region i,
V_i = volume of region i,
$P_{j\to i}(E)$ = collision probability for collision from region j to i,
$\sum_{s,i}(E'\to E)$ = macroscopic scattering cross section of region i from energy E' to E,
$\nu\sum_{f,i}(E)$ = macroscopic production cross section of region i,
$\chi_i(E)$ = fission spectrum of region i, and
$\phi_i(E)$ = neutron scalar flux of region i.

When the multi-group approximation is applied to Eq. (1), and assuming a constant neutron flux and cross section within a fine energy group, we have Eq. (2):

$$\Sigma_{t,f,fg}\phi_{f,fg}V_f=\sum_j P_{j\to f,fg}V_j\left(S_{j,fg}+\chi_{j,fg}\right), \quad (2)$$

where

fg = energy group index in ultra-fine group structure,
$\sum_{t,f,fg}$ = macroscopic total cross section of region f in group fg,
$\phi_{f,fg}$ = neutron scalar flux of region f in group fg,
V_f = volume of region f,
V_j = volume of region j,
$P_{j\to f,fg}$ = collision probability for collision from region j to region f in group fg,
$S_{j,fg}$ = scattering source of region j in group fg, and
$\chi_{j,fg}$ = fission spectrum of region j in group fg.

In the ultra-fine group method, the energy width for a fine group is set to be sufficiently small, satisfying the assumption of a constant cross section and neutron flux in the fine group. Typical lethargy widths in the ultra-fine group cross section library of the AEGIS code are 0.00005~0.00025 (for 5keV-1keV) and 0.0012~0.00029 (for 1keV-1eV), which are derived by the above discussion and sensitivity calculations.

When the scattering source is assumed to be dominated by the elastic scattering, the scattering source is given by Eq. (3):

$$S_{j,fg}=\sum_k\sum_{fg'}\frac{\Sigma_{es,j,k,fg'}\phi_{j,fg'}\Delta E_{fg'}}{(1-\alpha_k)\bar{E}_{fg'}}, \quad (3)$$

where

$\sum_{es,j,k,fg'}$ = macroscopic elastic scattering cross section for region j, nuclide k, group fg' ($=\sigma_{es,j,k,fg'}N_k$),
$\phi_{j,fg'}$ = neutron scalar flux at region j, group fg',
$\Delta E_{fg'}$ = energy width of group fg',
$\alpha_k=\left(\frac{A_k-1}{A_k+1}\right)^2$, where A_k is the mass number of the nuclide k, and
$\bar{E}_{fg'}$ = average energy of group fg'.

Eqs. (2) and (3) compose a recurrent relation on the energy groups. Thus, the above slowing down equation can be easily solved from higher energy to lower energy. It should be noted that the up-scatter of neutrons is not taken into account in the ultra-fine group calculation due to a computation time consideration. Instead, the energy group structure of the multi-group cross section library (XMAS structure) can directly handle the resonance at epithermal regions, i.e., the fine energy structure is adopted

for the important resonances of the heavy nuclides in epithermal to thermal energy ranges, e.g., 1.0eV resonance of ^{240}Pu and 0.3eV of ^{239}Pu.

Once the neutron spectrum in the ultra-fine group is obtained, the effective cross section of each nuclide is given by:

$$\sigma_{x,g} = \frac{\sum_{fg\in g} \phi_{f,fg}\sigma_{x,fg}}{\sum_{fg\in g} \phi_{f,fg}}, \quad (4)$$

where

$\sigma_{x,g}$ = microscopic effective cross section of multi-group g, reaction x, and

$\sigma_{x,fg}$ = microscopic cross section of ultra-fine group fg, reaction x.

Though Eq. (2) can be used for an arbitrary geometry, direct application to a whole fuel assembly is not practical due to computation time. Thus, the ultra-fine group spectrum calculation is applied at the pin-cell geometry in the AEGIS code. The treatment of position dependency of the effective cross section will be described in the next subsection.

The ultra-fine group calculation is sometimes performed in an approximated one-dimensional cylindrical geometry with the white boundary condition. However, based on the preliminary sensitivity calculations, the square shape of a fuel cell is explicitly treated in the AEGIS code in order to increase the accuracy of the effective cross section [6].

The collision probability calculation in the one-dimensional cylindrical geometry can be efficiently carried out, but that in a two-dimensional square-cell requires the ray trace approach and numerical integration, for which considerable computation time is necessary. Therefore, the collision probability in a fuel cell is pre-tabulated for various fuel, clad and moderator cross sections, and the collision probabilities are evaluated by the interpolation in the ultra-fine group calculations. This approach greatly contributes to reduction of computation time [6].

A further idea is also implemented to improve the calculation efficiency of the slowing down source in the ultra-fine group calculation of the AEGIS code. One of the most time-consuming parts in the ultra-fine group spectrum calculation is the slowing down source calculation, especially when light nuclides such as hydrogen are included. Therefore, the slowing down source in the moderator region is given as 1/E and no slowing down source calculation is carried out in the moderator region. Nuclides in pellet and cladding regions are classified into four categories according their mass, i.e., hydrogen (A=1), oxygen (A=16), other light to medium nuclides (A<90) and heavy nuclides (A≥90). By applying this grouping, the computation time for the slowing down calculation can be significantly reduced, since explicit consideration of the slowing down energy range for each nuclide can be avoided. The approximations used in the ultra-fine group calculations of the AEGIS code do not have significant impact on the accuracy of effective cross sections [6].

In a homogeneous system, the multi-group cross section given by Eq. (4) can exactly reproduce the reference reaction rate obtained in the ultra-fine group calculation. However, this is not true in a heterogeneous system because of the energy condensation error in the cross sections. Equation (4) implicitly assumes that the neutron flux obtained in a multi-group transport calculation, which utilizes the collapsed ultra-fine group cross section, is identical to the energy integrated value of the ultra-fine group flux. However, in reality, they are not identical due to the inability to retrieve the reference currents of the ultrafine group calculation.

In order to mitigate the error of the cross section condensation, the AEGIS code adopts the SPH method for energy condensation [6]. Reaction rates obtained by the multi-group transport calculation in a heterogeneous geometry can reproduce those obtained by the ultra-fine group spectrum calculation. The SPH method is applied by the following procedures:

1) Ultra-fine group spectrum calculation is carried out using Eq. (2) and then the effective cross section in multi-group (172 groups) structure is evaluated using Eq. (4).
2) A one-group transport calculation is carried out using the effective cross section obtained in (1) and the slowing down source for the multi-group structure is obtained in the ultra-fine group calculation.
3) The SPH factor is estimated using Eq.(5).

$$\mu_{i,g} = \frac{\sum_{fg\in g} \phi_{i,fg}}{\phi_{i,g}}, \quad (5)$$

where

$\mu_{i,g}$ = the SPH factor of region i, multi-group g,

$\phi_{i,fg}$ = neutron flux of region i, ultra-fine group fg, and

$\phi_{i,g}$ = neutron flux of region i, multi-group g.

4) The effective microscopic cross sections are corrected using Eq. (6).

$$\tilde{\sigma}_{i,x,g} = \sigma_{i,x,g}\mu_{i,g} \quad (6)$$

5) Steps (2) to (4) are repeated until the SPH factor converges.

By correcting the multi-group effective cross section, the reaction rate obtained in the multi-group transport calculation, i.e., $\tilde{\sigma}_{i,x,g}\phi_{i,g}$, becomes consistent with that of the reference reaction rate obtained by the ultra-fine group calculation, i.e., $\sum_{fg\in g}\phi_{f,fg}\sigma_{x,fg}$. This is clear from Eqs. (4), (5) and (6). The previous study suggests that the effect of the SPH factor in the energy condensation is approximately

0.3~0.4%Δk/k, which is not trivial [6].

The ultra-fine group calculation is applied not only to fuel cells, but also for control rod cells since the control rod material includes resonance nuclides such as Ag, In, and Cd [11].

2.2.3 Calculation of Position Dependent Effective Cross Section

In actual fuel assemblies, the effective cross sections at every fuel rod position are different due to the existence of guide thimbles, water holes, water gaps and so on. Therefore, the position dependency of the effective cross section should be taken into account in a fuel assembly calculation.

In the AEGIS code, the effective cross section in the resolved resonance energy range is calculated by the ultra-fine group method, but it is applied to only a unit fuel cell. Estimation of the position dependent effective cross section with the ultra-fine group method will be time consuming, since the ultra-fine group calculation should be repeatedly carried out for every fuel cell. In order to reduce computation time, the position dependent effective cross sections are evaluated through the Dancoff factor [12] in the AEGIS code.

First, the ultra-fine group spectrum calculations are carried out for each fuel cell type assuming three different ideal cell pitches. The relation between the Dancoff factor and the effective cross section can be pre-tabulated from these results. Then, the Dancoff factor for each fuel cell inside a fuel assembly is estimated by the neutron current method, which will be described later. Once the position dependent Dancoff factors are obtained, we can evaluate the position dependent effective cross section by interpolating the pre-tabulated table based on the relation between the Dancoff factor and the effective cross section. When there are multiple types of fuel cell in a fuel assembly, e.g., low, middle and high Pu content MOX fuel cells, the above procedure is repeatedly applied.

The present approach relies on the following two assumptions. First, the Dancoff factor is evaluated based on the black fuel assumption in which a very large cross section is used for fuel. In reality, the fuel cross section takes a different value in each energy group; thus, the Dancoff factor would be group dependent. Secondarily, relations between the Dancoff factor and the effective cross section are similar both in a fuel cell and in a fuel assembly. The validities of these two assumptions are confirmed through preliminary calculations that indicate a good and unified correlation among the Dancoff factors and the effective cross sections both for a fuel cell and a fuel assembly [13].

The Dancoff factor is evaluated by the neutron current method using MOC [14]. Though the Dancoff factor is traditionally evaluated by the collision probability method, it will require prohibitive computation time for a large geometry such as a fuel assembly or an entire core. Since the neutron current method utilizes MOC, it yields a position dependent Dancoff factor in a large and complicated geometry with a short computation time.

An original definition of the Dancoff factor is given by the ratio of numbers of incoming neutrons at the isolated and lattice geometries. When the fuel region is considered as black and no neutron source exists in the fuel region, neutron scalar flux at the fuel region and the number of neutrons coming into the fuel region have a proportional relationship. Therefore, we can evaluate the Dancoff factor by Eq. (7):

$$D = \frac{I}{I_0} = \frac{\phi}{\phi_0}, \tag{7}$$

where

I_0 = number of incoming neutrons into fuel region at an isolated system,

I = number of incoming neutrons into fuel region at an lattice system,

ϕ_0 = neutron flux in fuel region at an isolated system, and

ϕ = neutron flux in fuel region at an lattice system.

Equation (7) suggests that the Dancoff factor can be evaluated by the neutron scalar flux at the fuel region, which can be easily obtained by MOC.

The actual calculation procedure for the neutron current method is as follows:

1) Total cross sections for all regions except for fuel are assumed to be equal to the magnitude of the potential scattering cross section. Though the value of the potential scattering cross section is used for the total cross section, the scattering cross sections for all regions including fuel regions are assumed to be zero; i.e., the total cross section is equal to the absorption cross section in each region.
2) Neutron source intensity for all regions except for the fuel region is assumed to be the same as the magnitude of the potential scattering cross section, which is derived by the assumption of the narrow resonance approximation.
3) The total cross section of the fuel region is set to be a sufficiently large value, e.g., 10^5[1/cm], which represents the black assumption of fuel. The scattering cross section for the fuel region is set to be zero.
4) Neutron source intensity for the fuel region is set to zero at the fuel region.
5) One-group fixed source transport calculation is performed for an isolated system, in which the fuel region in question is put in a sufficiently large moderator.
6) Neutron scalar flux is estimated in step (5).
7) One-group fixed source transport calculation is performed for a lattice system, which corresponds to actual geometry.

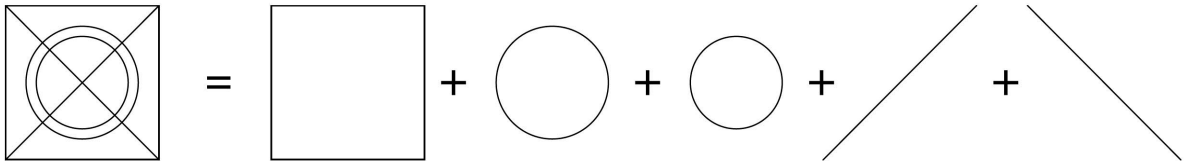

Fig. 1. Concept of Factorial Geometry

8) The neutron scalar flux of fuel regions is estimated in step (7)
9) The Dancoff factor is evaluated from the ratio of scalar neutron flux levels obtained in steps (6) and (8).

In the neutron current method, a one-group transport calculation without scattering is carried out. Since the asymptotic convergence rate of MOC is equal to the scattering ratio, the above calculation is efficiently carried out by MOC. Typically, one or two transport sweeps are sufficient to obtain a converged result; thus, computation time is short. For example, estimation of the Dancoff factor for each fuel pin in a two-dimensional whole PWR will require less than 10 seconds on an affordable PC by the neutron current method.

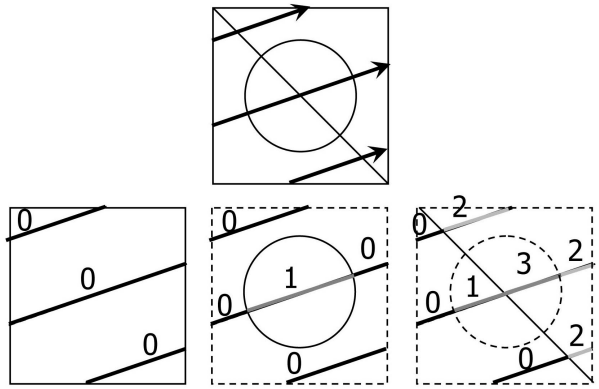

Fig. 2. Automated Generation of Region Number Index in Factorial Geometry

2.3 Assembly Transport Calculation

2.3.1 Overview

Once the effective cross section in each material has been generated, a transport calculation on the fuel assembly is carried out in an explicit heterogeneous geometry with the library energy group structure, i.e., 172 groups. This is one of the features of the AEGIS code. Neither energy condensation nor homogenization is carried out prior to the assembly transport calculation. Thus, errors due to energy condensation and homogenization can be avoided, contributing to accurate evaluation of the neutronics property of a highly heterogeneous fuel assembly.

The method of characteristics [15][16][17][18][19][20][21][22] is used for the assembly transport calculation due to its efficiency for handling a large and complicated geometry. Various numerical techniques are adopted for efficient execution of the assembly transport calculation, e.g., the ray tracing method, the acceleration method, and the polar angle quadrature set. In the following subsections, these numerical techniques are described.

2.3.2 Geometry Handling

Geometry handling is one of the most difficult issues in assembly transport calculation since various complicated geometries can appear in a fuel assembly. There are two approaches to address this issue. The first one is hard-coding, i.e., to prepare dedicated geometry routines in the transport calculation module. When the types of geometry which may appear in the target reactor types are limited, the first approach can be an efficient solution. The second approach is the utilization of a generalized geometry routine that can handle arbitrary geometries. Though the implementation of the second approach would be more difficult than that of the first approach, the second approach offers inherent flexibility in geometry handling.

The AEGIS code adopts the second approach. Two different numerical techniques are used, i.e., factorial geometry [23] for flux region definition and combinatorial geometry [24] with R-function [25] for material region definition.

The concept of factorial geometry is shown in Fig. 1. Factorial geometry represents a complicated figure by means of a combination of simple figures. In the AEGIS code, any combination of circles and lines can be treated, which allows the code to cover almost all geometries that appear in the fuel assembly of any reactor type.

One distinguished feature of factorial geometry is the automated generation of a region number index for each flat flux region, as shown in Fig. 2. The neutron flux and source are assumed to be constant in each flux region in the AEGIS code, which is a common treatment of MOC. Thus, a fine background mesh division would be necessary to suppress the spatial discretization error. Assigning region number indices to such fine background meshes is, of course, cumbersome. Factorial geometry offers a solution for this issue.

In the AEGIS code, the material region is assigned using combinatorial geometry, since fine background mesh division is not necessary for the material region. The concept of R-function is adopted to distinguish each region that can be defined by a mathematical equation, e.g., inside a circle.

The AEGIS code aims at handling not only a fuel assembly, but also larger and more complex shapes, such as the entire core of a commercial power reactor, in two-dimensional geometry. Since direct specification of geometry for such a large set of shapes requires considerable work, the repeated (lattice) geometry is adopted in two-levels, i.e., for the cell and fuel assembly. A fuel assembly can be specified as a repeated structure of unit cells, which are constructed from a combination of lines and circles. A core is then constructed from fuel assemblies. This approach has good affinity with the structure of the current power reactors, and preparation of input data is significantly simplified through this approach.

Since the AEGIS code can handle very complicated geometry, it has an auxiliary code, CLIP, which can plot the ray trace information in the AEGIS code. By using the CLIP code, one can easily check the validity of the assignment of flat flux and material regions.

2.3.3 Ray Trace

The ray trace method may have a significant impact on the calculation time and accuracy of a transport solver when using the method of characteristics. The AEGIS code utilizes the macroband method [26] for ray tracing of a unit cell and adopts non-uniform ray trace widths based on the Gauss-Legendre quadrature set [27].

The conventional macroband method puts equidistant ray traces between geometrically singular points such as intersection or tangential points. The spatial behavior of angular flux may be discontinuous at the singular points; thus, spatial integration of angular flux beyond the singular point can be a cause of significant spatial discretization error. Therefore, use of the macroband method can contribute to reduce the spatial discretization error of a coarse ray trace. The macroband method is applied at the unit cell level in the AEGIS code since direct application of the macroband method to a whole fuel assembly could result in overly narrow ray separation, due to the existence of many geometrically singular points inside a fuel assembly.

This approach also provides another way of increasing the efficiency of ray tracing: the memory reduction on macroband method, or MRMB [27]. In a common LWR fuel assembly, there are many cells with identical geometry. The ray trace information for a cell type can be repeatedly applied to all cells having identical geometry, which contributes to reducing memory storage and computation time.

In the conventional macroband method, ray separation

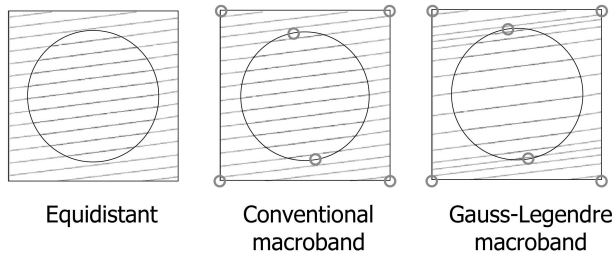

Fig. 3. Comparison of Ray Traces

is uniform between the geometrically singular points. However, in order to increase the accuracy of the spatial integration of the angular flux by the ray trace, non-uniform ray separation is applied as shown in Fig. 3. The weight (i.e., ray separation) and position of ray traces are chosen from the Gauss-Legendre quadrature set. Numerical integration using the Gauss-Legendre quadrature set of N-th order can exactly treat polynomials up to N+1-th order. Therefore, the accuracy of spatial integration can be increased if the spatial angular flux distribution is sufficiently smooth. As described above, since no singular point appears in the integrand, use of the Gauss-Legendre quadrature set has good affinity with the macroband method.

When the macroband method is applied for a unit cell, ray traces are not contiguous at the cell boundary. Therefore, the angular flux is linearly interpolated at cell boundaries in the AEGIS code.

2.3.3 Quadrature Set

In MOC, angular flux distributions along the azimuthal and polar directions are treated through discretization. Since the angular flux distribution for the azimuthal direction is very bumpy in heterogeneous geometry, a uniform angular division is applied for the azimuthal direction. However, for the polar direction, angular flux is rather smooth; thus, a dedicated quadrature set can reduce the discretization error for the polar direction [28][29][30] .

When isotropic scattering is assumed, the polar integrated angular flux calculation on a particular ray trace using MOC is equivalent to that using the collision probability method [30]. In the collision probability method, the polar angle integration is analytically carried out; thus, the collision probability is expressed with the Bickely-Naylor function in generalized two-dimensional geometry. On the other hand, angular integration for the polar direction is carried out through numerical integration with a specific quadrature set in MOC. Therefore, by choosing appropriate polar angles and their associated weights used for numerical integration that well reproduce the Bickley-Naylor function, the accuracy of MOC can be increased. Under this consideration, the optimized

quadrature set is derived by minimizing Eq. (8):

$$\left|Ki_n(x) - Ki_{An}(x)\right| = \left|\int_0^{\pi/2} d\theta \sin^{n-1}\theta \exp\left(-\frac{x}{\sin\theta}\right) - \sum_{m=1}^{N_0} \omega_m \sin^{n-2}\theta_m \exp\left(-\frac{x}{\sin\theta_m}\right)\right|, \quad (8)$$

where

$Ki_n(x)$ = the Bickley-Naylor function of n-th order,
$Ki_{An}(x)$ = the approximated Bickley-Naylor function using numerical integration,
θ = polar angle (measured from normal to two-dimensional plane),
ω_m = weight of the m-th polar angle,
θ_m = m-th polar angle, and
N_0 = number of divisions for polar angle. (N_0=1~3 in Ref. [30]).

The derived quadrature set for the polar angle, i.e., the Tabuchi-Yamamoto optimized quadrature set for the polar angle (TY-opt), is summarized in Table 1 [30]. The TY-opt quadrature set significantly reduces discretization error for the polar angle, and two polar angle divisions is commonly sufficient for LWR fuel assembly analysis.

2.3.4 Acceleration

The convergence of MOC is dominated by two ratios, i.e., the scattering ratio (the ratio of scattering to total cross sections) and the dominance ratio (the ratio of the first higher eigenvalue to the fundamental eigenvalue). In typical LWR applications, the scattering ratio is close to unity due to extensive scattering of the moderator material, and the dominance ratio may also be close to unity when a large configuration such as the entire core of a LWR is considered. Therefore, an acceleration method is necessary to obtain a converged flux solution within a practical computation time.

Table 1. Tabuchi-Yamamoto's Optimized Quadrature Set for Polar Angle (TY-opt.)

Number of polar divisions	sinθ[1)]	ω(weight)
1	0.798184	1.000000
2	0.363900	0.212854
	0.899900	0.787146
3	0.166648	0.046233
	0.537707	0.283619
	0.932954	0.670148

1) Angle (θ) is measured from z-axis.

In the AEGIS code, the generalized coarse mesh rebalance (GCMR) method is applied [31][32]. GCMR acceleration is a unified method of the coarse mesh rebalance (CMR) [33] and the coarse mesh finite difference (CMFD) accelerations [34][35][36][37][38]. In the GCMR method, the net neutron current between regions is given by Eq. (9):

$$J^i_{net,n,n+1} = -\alpha^i_n \phi^i_{s,n} + \beta^i_n \bar{\phi}_n, \quad (9)$$

where

i = transport sweep index,
n = mesh index,
$J^i_{net,n,n+1}$ = net neutron current between mesh n and $n+1$,
α^i_n, β^i_n = GCMR parameters,
$\phi^i_{s,n}$ = surface flux at region n, and
$\bar{\phi}_n$ = region average neutron flux.

Once α^i_n is fixed as a specific value, another coefficient β^i_n can be determined, since the neutron net current ($J^i_{net,n}$) and scalar fluxes ($\phi^i_{s,n}$, $\bar{\phi}_n$) are taken from MOC, though they may not be fully converged.

The similar relation for mesh n+1 is given by Eq. (10):

$$J^i_{net,n,n+1} = -\alpha^i_{n+1} \phi^i_{s,n+1} + \beta^i_{n+1} \bar{\phi}_{n+1}. \quad (10)$$

The parameter β^i_{n+1} can be determined through the same procedure for mesh n. Finally, applying the continuity condition for surface fluxes, i.e., $\phi^i_{s,n}=\phi^i_{s,n+1}$, the following relation can be obtained:

$$J^j_{net,n,n+1} = \frac{\alpha^i_n \beta^i_{n+1}}{\alpha^i_n + \alpha^i_{n+1}} \bar{\phi}_n - \frac{\alpha^i_{n+1} \beta^i_n}{\alpha^i_n + \alpha^i_{n+1}} \bar{\phi}_{n+1}. \quad (11)$$

Since Eq. (11) has a form consistent with that of a conventional differential equation, we can reconstruct a corrected finite-difference form for the neutron flux. By solving the corrected finite-difference equation, a better estimate for neutron flux for each region is obtained and the neutron scalar flux of each region in MOC is forced to match with this result (prolongation).

Choice of the acceleration parameter has significant impact on the convergence behavior. GCMR becomes identical to CMR when the value of α^i_n is $^1/_2$, while it is identical to CMFD when the value is $2D_n/\Delta h_n$, where D_n and Δh_n are the diffusion coefficient and the mesh width, respectively. Unfortunately, both methods have numerical instability for optically thin and/or thick mesh. In the AEGIS code, the initial value of α^i_n is set to be $2D_n/\Delta h_n$.

When the optical thickness of a mesh exceeds unity, α_n^i is set to be larger than $2D_n/\Delta h_n$ by multiplying a factor which is proportional to the optical thickness of the mesh. By applying GCMR, typically ten to twenty transport sweeps are sufficient to obtain converged results regardless of the size of the problem, i.e., from a pincell to an entire LWR core.

2.3.5 Anisotropic Scattering

In conventional lattice physics computation, implicit treatment of anisotropic scattering, i.e., the transport correction, is often used. However, for a highly heterogeneous fuel assembly such as MOX fuel, explicit treatment of anisotropic scattering is desirable for accurate prediction [5]. In the AEGIS code, the anisotropy of the scattering source is treated through the spherical harmonics expansion:

$$Q_{m,g} = \frac{1}{4\pi}\sum_{g'}\sum_{L}\sum_{M=-L}^{L}(2L+1)\Sigma_{sL,g'\to g}\phi_{L,M,g'}R_{L,M}(\vec{\Omega}_m), \quad (12)$$

where

$\phi_{L,M,g}$ = angular flux moment of (L,M)-th order in group g, and

$R_{L,M}(\vec{\Omega}_m)$= the real spherical harmonics function of (L,M)-th order.

Since the AEGIS code performs a transport calculation in two-dimensional geometry, the symmetry of the angular flux distribution for the upper and lower hemi-spheres is taken into account in order to suppress the number of expansion coefficients of angular flux distribution stored during a calculation. Only even moments of the angular flux are stored during computation when considering the symmetry.

2.4 Burnup Calculation

2.4.1 Overview

The burnup chain used in the AEGIS code consists of 28 heavy nuclides and 193 fission products, covering not only the U-Pu cycle but also the Th-U cycle. Very detailed treatment of fission products makes it possible to avoid treating lumped fission products[39].

In order to accurately handle the detailed burnup chain that has short-lived nuclides, a new burnup solver based on the Krylov subspace method is used in the AEGIS code [40]. Furthermore, the projected predictor-corrector method [41], which reduces discretization error resulting from using a constant reaction rate during a burnup step, is also developed and implemented in the AEGIS code. These two major numerical methods are described in the following sections.

2.4.2 Krylov Subspace Method for the Burnup Equation

Variation of nuclide number densities during burnup can be obtained by solving the following burnup equation in the AEGIS code.

$$\frac{dN_i}{dt} = \sum_j \gamma_{ji}\sigma_{f,j}N_j\phi + \sigma_{c,i-1}N_{i-1}\phi + \sigma_{n,2n,i+1}N_{i+1}\phi + \sum_k \lambda_k N_k - \sigma_{a,i}N_i\phi - \lambda_i N_i, \quad (13)$$

where

N_i = nuclide number density,

γ_{ji} = production of nuclide i through fission of nuclide j,

$\sigma_{f,j}$ = microscopic fission cross section of nuclide j,

ϕ = neutron flux,

$\sigma_{c,i-1}$ = microscopic capture cross section of nuclide i-1,

$\sigma_{n,2n,i+1}$ = microscopic (n,2n) cross section of nuclide i+1, and

$\sigma_{a,i}$ = microscopic absorption cross section of nuclide i.

The burnup equation given by Eq. (13) has a first-order differential form in time. When the number densities are treated as a vector, Eq. (13) can be re-written as Eq. (14), which is in a more general form:

$$\frac{d\vec{N}}{dt} = \mathbf{A}\vec{N}, \quad (14)$$

where

$\vec{N}$ = vector of nuclide number densities appearing in the burnup equation, and

$\mathbf{A}$ = burnup matrix whose elements are coefficients of the burnup equation.

The solution of Eq. (14) is given by the following analytical form:

$$\vec{N}(t+\Delta t) = \exp(\mathbf{A}\Delta t)\vec{N}(t), \quad (15)$$

where

$\exp(\mathbf{A}\Delta t)$ is a matrix exponential.

Various numerical methods can be used to evaluate the matrix exponential [42]. However, when the disintegration rate (decay and/or absorption rate) of a nuclide is very large, the norm of the burnup matrix becomes large, resulting in serious round-off error due to poor convergence behavior of the Taylor series expansion of the matrix exponential. Many conventional numerical methods, e.g., the matrix exponential method [43] and the fourth-order Runge-Kutta method, rely on the Taylor series expansion; thus, direct utilization of these methods

may suffer from a numerical problem due to the round-off error. In such cases, use of the scaling and squaring method and/or the analytical solution assuming an equilibrium state may be in order [43].

In the AEGIS code, the matrix exponential of the burnup equation is directly evaluated by the Krylov subspace method [40]. The rough concept and procedure of this method is summarized as follows:

1) The predicted number density at the next burnup step, i.e., $\exp(\mathbf{A}\Delta t)\vec{N}(t)$, is expanded with the Krylov subspace, which is a set of vectors defined by $\{\vec{N}(t), (\mathbf{A}\Delta t)\vec{N}(t), (\mathbf{A}\Delta t)^2\vec{N}(t), ..., (\mathbf{A}\Delta t)^{m-1}\vec{N}(t)\}$, and then the expansion coefficients are obtained by a numerical procedure shown in Ref. [40].
2) Using the coefficients obtained in step (1), the burnup matrix, which is sparse, is converted into a smaller dense matrix.
3) The matrix exponential of the small dense matrix obtained in Step (2) is evaluated.
4) Using the matrix exponential of the small dense matrix and the Krylov subspace, the number density at the next step is evaluated.

The Krylov subspace method is particularly effective in solving the burnup equation since the original burnup matrix is very sparse. In the AEGIS code, the rank of the original burnup matrix is more than two hundred, but it is compressed to a small dense matrix whose rank is approximately 20~30. Since the matrix exponential is calculated only for this small matrix, the present method offers a computationally efficient approach to evaluate Eq. (15).

2.4.3 Projected Predictor-Corrector Method

There are two different sources of discretization error in the numerical calculation of the burnup equation. The first one is the temporal discretization and the second one is the use of a constant reaction rate during a burnup step. The AEGIS code is almost free from the former discretization error due to the incorporation of the Krylov subspace method. However, the latter, i.e., the assumption of a constant reaction rate, should still be taken into account.

The assumption of a constant reaction rate may cause a significant error when the microscopic reaction rate rapidly changes with burnup. In LWR analysis, Gadolinia bearing fuel causes such a situation until the Gadolinium isotopes are burned out. In order to overcome the rapid variation of the microscopic reaction rate, the predictor-corrector (PC) method is commonly incorporated in common lattice physics codes. Though the PC method is very effective, the typical burnup step required for a Gadolinia bearing fuel assembly is 0.2GWd/t; thus, a few hundred steps are still necessary to deplete it.

In the conventional PC method, the number density used in the corrector step is obtained by means of the depletion calculation with the microscopic reaction rate estimated in the predictor step. Thus, the number density used at the corrector step may be "under-depleted" in the case of Gadolinium bearing fuel pellets, since the microscopic reaction rate rapidly increases with burnup at the beginning of life through the middle of life. Consequently, the microscopic reaction rate obtained in the corrector step is also underestimated. Since the reaction rates in the predictor and corrector steps are both underestimated, the estimated final number density inevitably contains error.

In the AEGIS code, the projected predictor-corrector (PPC) method is implemented to mitigate the above assumption [41]. The PPC method utilizes a relationship between the number density and the microscopic reaction rate for a nuclide to make a projection of the microscopic reaction rate at the adequate burnup point. The actual calculation procedure of the PPC method is as follows:

1) The microscopic effective cross section of each nuclide is evaluated at burnup step n with the number density (N_n). The two-dimensional transport calculation is carried out with the evaluated macroscopic effective cross section, followed by the estimation of the microscopic reaction rate of each nuclide. The estimated microscopic reaction rate is used to obtain the predictor number density (N^p_{n+1}) at the next burnup step n+1.
2) The microscopic reaction rate of each nuclide at burnup step n+1 is estimated with the predicted number density (N^p_{n+1}), which is similar to the procedure in step (1). The corrector number density (N^c_{n+1}) at step n+1 is evaluated using the microscopic reaction rate obtained in this step. In the conventional PC method, the average of the predictor and corrector number densities (N^p_{n+1}+N^c_{n+1})/2 is used as the final number density of step n+1.
3) The "effective" microscopic reaction rates, i.e., R^p and R^c, are calculated by Eqs. (16) and (17).

$$R^p = -\ln(N^p_{n+1} / N_n), \text{ and} \tag{16}$$

$$R^c = -\ln(N^c_{n+1} / N_n). \tag{17}$$

4) The effective microscopic reaction rates (R^p and R^c) are obtained with the number densities N_n (predictor step) and N^p_{n+1} (corrector step), respectively. Since there is a fairly good linear correlation between the number density and the corresponding microscopic reaction rate, the effective microscopic reaction rate for arbitrary number density N can be given by:

$$R = \frac{R^p - R^c}{N_n - N^p_{n+1}}(N - N^p_{n+1}) + R^c. \tag{18}$$

5) The best estimated number density at the corrector step so far is $N=(N^{p}_{n+1}+N^{c}_{n+1})/2$; thus, a more accurate microscopic reaction rate at the corrector step is given by Eq. (19), by substituting $N=(N^{p}_{n+1}+N^{c}_{n+1})/2$ into Eq. (18):

$$R^{c,\mathrm{mod}}=\frac{R^{p}-R^{c}}{N_{n}-N^{p}_{n+1}}[(N^{p}_{n+1}+N^{c}_{n+1})/2-N^{p}_{n+1}]+R^{c}. \quad (19)$$

6) By using $R^{c,\mathrm{mod}}$, a more accurate corrector number density is given by:

$$N^{c,\mathrm{mod}}_{n+1}=N_{n}\exp(-R^{c,\mathrm{mod}}). \quad (20)$$

7) Finally, the number density at step n+1 is given by Eq. (21):

$$N_{n+1}=\left(N^{p}_{n+1}+N^{c,\mathrm{mod}}_{n+1}\right)/2. \quad (21)$$

Since the number of assembly transport calculations, which is a dominant part of computation time, is equivalent to that in the PC method, and because additional computation for the PPC method is trivial, the PPC method is computationally efficient. Though the PPC method can be applied to every nuclide, it is applied to only Gadolinium isotopes in the AEGIS code based on preliminary sensitivity analysis. The conventional PC method is used for other nuclides.

By adopting the PPC method, the number of burnup steps to deplete a Gadolinium bearing fuel assembly is at least halved. In other words, the burnup step size can be increased at least two times without loss of accuracy.

3. VERIFICATIONS

In this section, typical verification results of the AEGIS code are presented. Due to the complexity of a lattice physics code, the verification results of major calculation capabilities, i.e., transport, effective cross section and burnup calculations, will be described followed by the analysis result of critical experiments which shows the soundness of the whole calculation by AEGIS.

3.1 Transport Solver

The C5G7 benchmark problem is analyzed in order to confirm the validity of the transport solver of the AEGIS code, which is based on MOC [44]. The C5G7 benchmark problem consists of two UO_2 and two MOX PWR heterogeneous fuel assemblies surrounded by water reflectors, as shown in Fig. 4. The cross sections for seven groups for each material and geometry specified in the benchmark problem are used in the present calculation. Though the reference result obtained with the MCNP code with 300 million histories is provided for the C5G7 benchmark problem, a new reference solution is evaluated using an in-house multi-group Monte-Carlo code, which adopts the track length estimator, with 10 billion histories in order to reduce the statistical error and perform a more precise comparison.

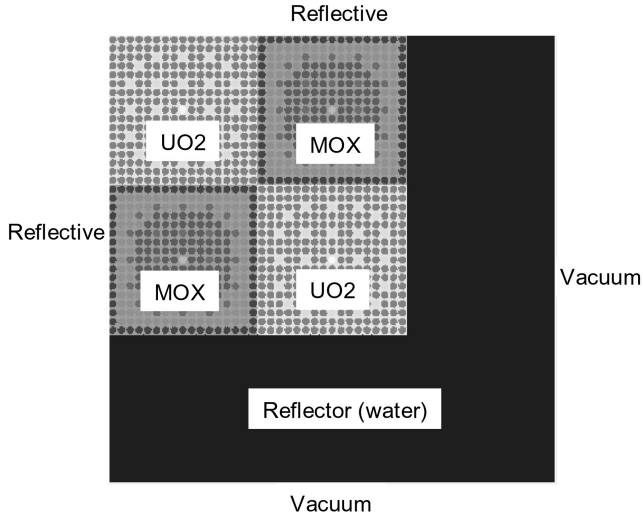

Fig. 4. Configuration of C5G7 Benchmark Problem

Calculation conditions used in the AEGIS code are as follows and are defined by the sensitivity analyses on the discretization parameters:

- Ray separation: less than 0.02cm using the Gauss-Legendre macroband method
- Number of azimuthal angles: 128 (for 2π)
- Number of polar angles: 3 (for $\pi/2$ using the TY-opt quadrature set)
- Background mesh: fuel and reflector cells (1.26cm× 1.26cm) are divided into 20×20 meshes in addition to the material boundary

A comparison of pin-by-pin fission rates between the in-house Monte-Carlo code (reference) and the AEGIS code is shown in Figs. 5-7. The root mean square and maximum errors of the pin-by-pin fission rate of the AEGIS code are 0.05% and 0.25%, respectively, for the whole C5G7 benchmark configuration. The difference between the k-effective of the reference and the AEGIS code is 0.001%.

The present result indicates that the transport solver of the AEGIS code can provide an accurate solution for complicated two-dimensional heterogeneous geometry problems.

2.1975	2.2023	2.2114	2.2234	2.2278	2.2294	2.1846	2.1473	2.1194	2.0548	1.9985	1.9483	1.8550	1.7530	1.6316	1.4840	1.2811
2.1982	2.2025	2.2120	2.2238	2.2279	2.2302	2.1856	2.1480	2.1197	2.0563	1.9995	1.9487	1.8555	1.7534	1.6325	1.4841	1.2814
-0.03%	-0.01%	-0.03%	-0.02%	0.00%	-0.04%	-0.05%	-0.04%	-0.01%	-0.07%	-0.05%	-0.02%	-0.03%	-0.02%	-0.05%	-0.01%	-0.02%
2.2023	2.2138	2.2387	2.2750	2.3030	2.3717	2.2538	2.2130	2.2492	2.1185	2.0610	2.0726	1.9190	1.7953	1.6534	1.4924	1.2812
2.2019	2.2141	2.2385	2.2755	2.3029	2.3728	2.2543	2.2140	2.2499	2.1192	2.0617	2.0735	1.9193	1.7955	1.6539	1.4929	1.2818
0.02%	-0.01%	0.01%	-0.02%	0.00%	-0.05%	-0.02%	-0.04%	-0.03%	-0.03%	-0.03%	-0.04%	-0.01%	-0.01%	-0.03%	-0.03%	-0.04%
2.2114	2.2387	2.3118	2.4428	2.4709		2.3828	2.3351		2.2366	2.1774		2.0604	1.9302	1.7115	1.5116	1.2852
2.2114	2.2402	2.3123	2.4437	2.4718		2.3836	2.3355		2.2373	2.1778		2.0610	1.9311	1.7120	1.5121	1.2860
0.00%	-0.06%	-0.02%	-0.04%	-0.04%		-0.03%	-0.02%		-0.03%	-0.02%		-0.03%	-0.05%	-0.03%	-0.03%	-0.06%
2.2234	2.2750	2.4428		2.4982	2.4557	2.2947	2.2449	2.2911	2.1492	2.0977	2.1444	2.0789		1.8129	1.5397	1.2927
2.2234	2.2760	2.4436		2.4993	2.4567	2.2951	2.2450	2.2911	2.1494	2.0978	2.1450	2.0797		1.8139	1.5401	1.2936
0.00%	-0.05%	-0.03%		-0.04%	-0.04%	-0.02%	0.00%	0.00%	-0.01%	-0.01%	-0.03%	-0.04%		-0.06%	-0.03%	-0.07%
2.2278	2.3030	2.4709	2.4982	2.4018	2.4273	2.2784	2.2312	2.2777	2.1365	2.0837	2.1213	2.0008	1.9729	1.8324	1.5613	1.2971
2.2277	2.3032	2.4718	2.4998	2.4031	2.4288	2.2784	2.2310	2.2777	2.1362	2.0838	2.1216	2.0013	1.9729	1.8327	1.5619	1.2982
0.00%	-0.01%	-0.03%	-0.06%	-0.06%	-0.06%	0.00%	0.01%	0.00%	0.01%	0.00%	-0.02%	-0.02%	0.00%	-0.02%	-0.04%	-0.09%
2.2294	2.3717		2.4557	2.4273		2.3474	2.3011		2.2052	2.1471		2.0263	1.9394		1.6127	1.3010
2.2296	2.3727		2.4569	2.4280		2.3481	2.3015		2.2056	2.1477		2.0268	1.9398		1.6130	1.3018
-0.01%	-0.04%		-0.05%	-0.03%		-0.03%	-0.02%		-0.02%	-0.03%		-0.02%	-0.02%		-0.02%	-0.06%
2.1846	2.2538	2.3828	2.2947	2.2784	2.3474	2.2174	2.1771	2.2250	2.0860	2.0307	2.0559	1.9033	1.8148	1.7682	1.5314	1.2761
2.1850	2.2539	2.3829	2.2946	2.2781	2.3480	2.2181	2.1766	2.2255	2.0856	2.0303	2.0565	1.9037	1.8152	1.7685	1.5318	1.2765
-0.02%	-0.01%	0.00%	0.01%	0.01%	-0.02%	-0.03%	0.02%	-0.02%	0.02%	0.02%	-0.03%	-0.02%	-0.02%	-0.02%	-0.02%	-0.03%
2.1473	2.2130	2.3351	2.2449	2.2312	2.3011	2.1771	2.1389	2.1857	2.0502	1.9955	2.0179	1.8667	1.7784	1.7359	1.5068	1.2574
2.1475	2.2137	2.3354	2.2452	2.2315	2.3017	2.1776	2.1391	2.1863	2.0507	1.9960	2.0180	1.8668	1.7783	1.7368	1.5068	1.2576
-0.01%	-0.03%	-0.01%	-0.01%	-0.01%	-0.03%	-0.03%	-0.01%	-0.03%	-0.02%	-0.02%	-0.01%	0.00%	0.00%	-0.05%	0.00%	-0.01%
2.1194	2.2492		2.2911	2.2777		2.2250	2.1857		2.0972	2.0401		1.9100	1.8180		1.5389	1.2461
2.1197	2.2497		2.2910	2.2774		2.2262	2.1864		2.0972	2.0409		1.9102	1.8182		1.5392	1.2463
-0.02%	-0.02%		0.01%	0.01%		-0.05%	-0.03%		0.00%	-0.04%		-0.01%	-0.01%		-0.02%	-0.02%
2.0548	2.1185	2.2366	2.1492	2.1365	2.2052	2.0860	2.0502	2.0972	1.9670	1.9154	1.9390	1.7938	1.7101	1.6717	1.4516	1.2122
2.0552	2.1181	2.2374	2.1491	2.1366	2.2053	2.0859	2.0502	2.0975	1.9675	1.9158	1.9397	1.7939	1.7104	1.6716	1.4517	1.2124
-0.02%	0.02%	-0.04%	0.00%	0.00%	0.00%	0.01%	0.00%	-0.02%	-0.02%	-0.02%	-0.04%	-0.01%	-0.02%	0.00%	0.00%	-0.02%
1.9985	2.0610	2.1774	2.0977	2.0837	2.1471	2.0307	1.9955	2.0401	1.9154	1.8666	1.8908	1.7534	1.6744	1.6339	1.4187	1.1851
1.9984	2.0616	2.1782	2.0985	2.0839	2.1474	2.0310	1.9954	2.0417	1.9156	1.8669	1.8916	1.7538	1.6748	1.6342	1.4185	1.1856
0.01%	-0.03%	-0.04%	-0.04%	-0.01%	-0.01%	-0.01%	0.01%	-0.08%	-0.01%	-0.01%	-0.04%	-0.02%	-0.03%	-0.02%	0.02%	-0.04%
1.9483	2.0726		2.1444	2.1213		2.0559	2.0179		1.9390	1.8908		1.7904	1.7175		1.4378	1.1639
1.9488	2.0729		2.1450	2.1216		2.0564	2.0181		1.9397	1.8915		1.7916	1.7178		1.4384	1.1640
-0.03%	-0.01%		-0.03%	-0.02%		-0.03%	-0.01%		-0.04%	-0.03%		-0.06%	-0.02%		-0.04%	-0.01%
1.8550	1.9190	2.0604	2.0789	2.0008	2.0263	1.9033	1.8667	1.9100	1.7938	1.7534	1.7904	1.6920	1.6735	1.5637	1.3380	1.1169
1.8551	1.9190	2.0602	2.0794	2.0010	2.0266	1.9038	1.8672	1.9099	1.7944	1.7535	1.7907	1.6915	1.6728	1.5640	1.3389	1.1168
-0.01%	0.00%	0.01%	-0.02%	-0.01%	-0.02%	-0.03%	-0.03%	0.00%	-0.03%	-0.01%	-0.01%	0.03%	0.04%	-0.02%	-0.06%	0.00%
1.7530	1.7953	1.9302		1.9729	1.9394	1.8148	1.7784	1.8180	1.7101	1.6744	1.7175	1.6735		1.4768	1.2623	1.0679
1.7531	1.7958	1.9309		1.9727	1.9397	1.8149	1.7787	1.8180	1.7106	1.6742	1.7184	1.6739		1.4771	1.2624	1.0680
-0.01%	-0.03%	-0.04%		0.01%	-0.02%	-0.01%	-0.02%	0.00%	-0.03%	0.01%	-0.06%	-0.03%		-0.02%	-0.01%	-0.01%
1.6316	1.6534	1.7115	1.8129	1.8324		1.7682	1.7359		1.6717	1.6339		1.5637	1.4768	1.3186	1.1758	1.0134
1.6320	1.6537	1.7118	1.8133	1.8327		1.7689	1.7369		1.6723	1.6343		1.5646	1.4769	1.3187	1.1760	1.0135
-0.02%	-0.02%	-0.02%	-0.02%	-0.02%		-0.04%	-0.05%		-0.04%	-0.03%		-0.06%	0.00%	0.00%	-0.01%	-0.01%
1.4840	1.4924	1.5116	1.5397	1.5613	1.6127	1.5314	1.5068	1.5389	1.4516	1.4187	1.4378	1.3380	1.2623	1.1758	1.0807	0.9541
1.4841	1.4930	1.5115	1.5399	1.5614	1.6134	1.5320	1.5069	1.5393	1.4516	1.4186	1.4380	1.3384	1.2622	1.1756	1.0805	0.9542
-0.01%	-0.04%	0.01%	-0.01%	-0.01%	-0.05%	-0.04%	-0.01%	-0.03%	0.00%	0.01%	-0.02%	-0.02%	0.01%	0.02%	0.02%	-0.01%
1.2811	1.2812	1.2852	1.2927	1.2971	1.3010	1.2761	1.2574	1.2461	1.2122	1.1851	1.1639	1.1169	1.0679	1.0134	0.9541	0.8782
1.2816	1.2816	1.2853	1.2928	1.2974	1.3013	1.2762	1.2572	1.2464	1.2123	1.1851	1.1641	1.1166	1.0673	1.0127	0.9541	0.8783
-0.04%	-0.03%	-0.01%	-0.01%	-0.03%	-0.02%	-0.01%	0.02%	-0.02%	-0.01%	0.00%	-0.02%	0.02%	0.05%	0.06%	0.00%	-0.02%

Fig. 5. Comparison of Pin-by-pin Fission Rate at Inner UO_2 Fuel Assembly
(Upper: AEGIS, Middle: Monte-Carlo, Lower: (AE-MC)/MC)

1.3127	1.2958	1.2896	1.2918	1.2946	1.2961	1.2736	1.2553	1.2428	1.2116	1.1856	1.1642	1.1214	1.0776	1.0355	1.0061	1.0129
1.3129	1.2958	1.2895	1.2918	1.2950	1.2963	1.2733	1.2550	1.2426	1.2113	1.1854	1.1641	1.1213	1.0778	1.0355	1.0062	1.0121
-0.02%	0.00%	0.01%	0.00%	-0.03%	-0.02%	0.02%	0.02%	0.02%	0.03%	0.02%	0.01%	0.00%	-0.02%	0.00%	-0.01%	0.08%
1.0625	1.3428	1.3205	1.3325	1.3589	1.4243	1.3325	1.3114	1.3614	1.2684	1.2432	1.2856	1.1870	1.1254	1.0832	1.0909	0.9093
1.0626	1.3431	1.3207	1.3326	1.3584	1.4245	1.3323	1.3119	1.3617	1.2680	1.2436	1.2855	1.1866	1.1252	1.0825	1.0902	0.9093
-0.01%	-0.02%	-0.01%	-0.01%	0.03%	-0.02%	0.01%	-0.03%	-0.02%	0.03%	-0.03%	0.01%	0.03%	0.02%	0.06%	0.06%	0.00%
0.9372	1.1711	1.1778	1.2628	1.2890		1.2234	1.1994		1.1636	1.1422		1.1351	1.0795	0.9854	0.9852	0.8549
0.9372	1.1712	1.1778	1.2636	1.2890		1.2232	1.1996		1.1639	1.1424		1.1351	1.0796	0.9854	0.9850	0.8543
0.00%	-0.01%	0.00%	-0.06%	0.00%		0.01%	-0.02%		-0.02%	-0.02%		0.00%	-0.01%	0.00%	0.02%	0.07%
0.8649	1.0938	1.1752		1.1817	1.2799	1.1471	1.1235	1.1896	1.0897	1.0747	1.1624	1.0418		0.9975	0.9413	0.8187
0.8650	1.0937	1.1759		1.1814	1.2800	1.1469	1.1240	1.1901	1.0898	1.0744	1.1624	1.0415		0.9974	0.9409	0.8182
0.00%	0.00%	-0.05%		0.03%	-0.01%	0.01%	-0.04%	-0.04%	-0.01%	0.03%	0.00%	0.03%		0.01%	0.04%	0.06%
0.8130	1.0484	1.1193	1.1125	1.1442	1.1428	1.0382	1.0185	1.0736	0.9890	0.9756	1.0428	1.0148	0.9630	0.9584	0.9158	0.7869
0.8131	1.0488	1.1196	1.1128	1.1441	1.1432	1.0381	1.0190	1.0745	0.9887	0.9752	1.0431	1.0141	0.9632	0.9584	0.9160	0.7866
-0.01%	-0.03%	-0.03%	-0.03%	0.01%	-0.04%	0.01%	-0.04%	-0.08%	0.03%	0.04%	-0.03%	0.07%	-0.03%	0.00%	-0.02%	0.04%
0.7691	1.0451		1.1281	1.0838		1.0371	1.0179		0.9912	0.9754		0.9687	0.9820		0.9221	0.7560
0.7694	1.0451		1.1281	1.0836		1.0369	1.0182		0.9908	0.9751		0.9689	0.9819		0.9216	0.7561
-0.04%	0.00%		0.00%	0.02%		0.02%	-0.03%		0.04%	0.02%		-0.02%	0.00%		0.06%	-0.02%
0.7136	0.9191	0.9505	0.9578	0.9288	0.9849	0.9003	0.8869	0.9438	0.8633	0.8500	0.9054	0.8331	0.8390	0.8249	0.8195	0.7105
0.7137	0.9190	0.9506	0.9578	0.9288	0.9848	0.9003	0.8868	0.9440	0.8632	0.8501	0.9056	0.8331	0.8389	0.8251	0.8194	0.7106
-0.01%	0.02%	-0.01%	0.00%	0.00%	0.01%	0.01%	0.02%	-0.02%	0.01%	-0.01%	-0.01%	-0.01%	0.02%	-0.02%	0.01%	-0.01%
0.6641	0.8509	0.8704	0.8808	0.8555	0.9022	0.8330	0.8220	0.8686	0.8008	0.7885	0.8327	0.7709	0.7763	0.7615	0.7656	0.6684
0.6641	0.8505	0.8703	0.8807	0.8554	0.9021	0.8330	0.8220	0.8686	0.8007	0.7885	0.8326	0.7708	0.7762	0.7615	0.7657	0.6682
0.00%	0.05%	0.01%	0.02%	0.01%	0.01%	0.00%	0.01%	0.00%	0.02%	0.01%	0.01%	0.01%	0.02%	0.00%	-0.01%	0.03%
0.6213	0.8395		0.8767	0.8534		0.8336	0.8221		0.8028	0.7895		0.7732	0.7763		0.7600	0.6310
0.6215	0.8393		0.8767	0.8536		0.8341	0.8223		0.8024	0.7897		0.7730	0.7767		0.7600	0.6311
-0.03%	0.03%		0.00%	-0.02%		-0.06%	-0.03%		0.05%	-0.03%		0.02%	-0.05%		0.00%	-0.01%
0.5706	0.7335	0.7561	0.7597	0.7383	0.7857	0.7203	0.7113	0.7585	0.6943	0.6842	0.7290	0.6703	0.6759	0.6689	0.6694	0.5844
0.5703	0.7332	0.7564	0.7598	0.7384	0.7854	0.7202	0.7116	0.7583	0.6941	0.6843	0.7287	0.6700	0.6758	0.6687	0.6693	0.5839
0.06%	0.04%	-0.04%	-0.02%	-0.01%	0.04%	0.01%	-0.04%	0.02%	0.04%	-0.01%	0.04%	0.05%	0.01%	0.02%	0.02%	0.08%
0.5249	0.6729	0.6890	0.6986	0.6781	0.7144	0.6600	0.6517	0.6889	0.6365	0.6281	0.6646	0.6176	0.6244	0.6132	0.6181	0.5417
0.5247	0.6726	0.6893	0.6985	0.6781	0.7141	0.6599	0.6518	0.6890	0.6364	0.6281	0.6648	0.6176	0.6246	0.6132	0.6177	0.5413
0.04%	0.04%	-0.04%	0.01%	0.00%	0.04%	0.01%	-0.01%	0.00%	0.02%	0.00%	-0.02%	0.00%	-0.03%	0.00%	0.06%	0.08%
0.4848	0.6576		0.7032	0.6780		0.6540	0.6442		0.6305	0.6224		0.6201	0.6309		0.6063	0.5035
0.4847	0.6572		0.7031	0.6783		0.6546	0.6445		0.6302	0.6222		0.6199	0.6310		0.6059	0.5033
0.02%	0.06%		0.01%	-0.04%		-0.09%	-0.04%		0.04%	0.04%		0.02%	-0.02%		0.08%	0.05%
0.4386	0.5674	0.6073	0.5891	0.6107	0.6207	0.5615	0.5528	0.5898	0.5407	0.5356	0.5793	0.5588	0.5305	0.5450	0.5266	0.4588
0.4386	0.5671	0.6070	0.5890	0.6111	0.6209	0.5616	0.5528	0.5896	0.5407	0.5354	0.5796	0.5587	0.5306	0.5452	0.5261	0.4588
-0.01%	0.06%	0.05%	0.01%	-0.07%	-0.04%	-0.02%	0.00%	0.05%	-0.01%	0.03%	-0.06%	0.02%	-0.03%	-0.04%	0.10%	0.00%
0.3989	0.5045	0.5426		0.5384	0.5775	0.5219	0.5129	0.5412	0.5018	0.4985	0.5398	0.4932		0.4891	0.4707	0.4200
0.3992	0.5040	0.5426		0.5384	0.5772	0.5218	0.5126	0.5408	0.5011	0.4984	0.5399	0.4931		0.4889	0.4709	0.4198
-0.08%	0.11%	0.00%		0.00%	0.05%	0.02%	0.07%	0.07%	0.14%	0.01%	-0.03%	0.02%		0.03%	-0.05%	0.05%
0.3778	0.4704	0.4753	0.5137	0.5183		0.4886	0.4806		0.4709	0.4667		0.4769	0.4651	0.4292	0.4394	0.3975
0.3777	0.4702	0.4750	0.5134	0.5180		0.4885	0.4808		0.4709	0.4667		0.4765	0.4651	0.4292	0.4394	0.3973
0.02%	0.04%	0.07%	0.06%	0.06%		0.02%	-0.03%		0.01%	0.01%		0.07%	0.02%	0.00%	0.01%	0.05%
0.4101	0.5165	0.5079	0.5133	0.5237	0.5500	0.5146	0.5085	0.5318	0.4980	0.4926	0.5159	0.4823	0.4653	0.4579	0.4779	0.4208
0.4095	0.5163	0.5075	0.5130	0.5230	0.5495	0.5147	0.5085	0.5315	0.4981	0.4925	0.5156	0.4823	0.4654	0.4577	0.4775	0.4205
0.16%	0.05%	0.09%	0.07%	0.13%	0.10%	-0.03%	0.00%	0.05%	-0.03%	0.02%	0.07%	0.00%	-0.01%	0.05%	0.10%	0.09%
0.6001	0.5923	0.5885	0.5878	0.5881	0.5880	0.5811	0.5758	0.5724	0.5638	0.5570	0.5521	0.5416	0.5323	0.5276	0.5358	0.5762
0.5992	0.5919	0.5884	0.5876	0.5874	0.5877	0.5811	0.5756	0.5724	0.5636	0.5566	0.5517	0.5414	0.5320	0.5272	0.5353	0.5758
0.16%	0.08%	0.01%	0.04%	0.11%	0.05%	0.01%	0.05%	0.01%	0.02%	0.06%	0.08%	0.04%	0.06%	0.08%	0.09%	0.07%

Fig. 6. Comparison of Pin-by-pin Fission Rate at Lower Left MOX Fuel Assembly
(Upper: AEGIS, Middle: Monte-Carlo, Lower: (AE-MC)/MC)

0.7948	0.7905	0.7722	0.7508	0.7261	0.7002	0.6596	0.6219	0.5881	0.5451	0.5059	0.4710	0.4297	0.3949	0.3743	0.3908	0.5022
0.7948	0.7907	0.7726	0.7507	0.7261	0.7003	0.6598	0.6220	0.5883	0.5450	0.5055	0.4709	0.4295	0.3947	0.3741	0.3902	0.5016
0.00%	-0.03%	-0.05%	0.02%	0.00%	0.00%	-0.03%	-0.02%	-0.03%	0.02%	0.07%	0.02%	0.07%	0.06%	0.05%	0.14%	0.12%
0.7905	0.8271	0.8316	0.8260	0.8113	0.8083	0.7399	0.6974	0.6804	0.6131	0.5692	0.5475	0.4864	0.4428	0.4144	0.4250	0.5286
0.7902	0.8269	0.8318	0.8261	0.8110	0.8078	0.7399	0.6975	0.6803	0.6128	0.5687	0.5472	0.4866	0.4427	0.4141	0.4247	0.5282
0.04%	0.03%	-0.02%	-0.01%	0.03%	0.06%	-0.01%	-0.01%	0.02%	0.06%	0.09%	0.06%	-0.04%	0.02%	0.09%	0.07%	0.08%
0.7722	0.8316	0.8646	0.8995	0.8867		0.8011	0.7536		0.6648	0.6170		0.5369	0.4896	0.4404	0.4391	0.5347
0.7720	0.8313	0.8645	0.8996	0.8863		0.8012	0.7535		0.6646	0.6167		0.5368	0.4894	0.4401	0.4387	0.5343
0.02%	0.04%	0.01%	-0.02%	0.04%		-0.01%	0.02%		0.04%	0.04%		0.03%	0.04%	0.07%	0.09%	0.07%
0.7508	0.8260	0.8995		0.8916	0.8513	0.7683	0.7229	0.7094	0.6377	0.5942	0.5812	0.5404		0.4655	0.4444	0.5310
0.7511	0.8258	0.8992		0.8916	0.8507	0.7678	0.7229	0.7095	0.6374	0.5941	0.5808	0.5402		0.4652	0.4439	0.5306
-0.03%	0.02%	0.03%		0.01%	0.06%	0.07%	0.01%	-0.01%	0.03%	0.03%	0.06%	0.04%		0.07%	0.11%	0.07%
0.7261	0.8113	0.8867	0.8916	0.8392	0.8243	0.7488	0.7062	0.6931	0.6240	0.5815	0.5664	0.5135	0.4932	0.4635	0.4423	0.5208
0.7265	0.8112	0.8862	0.8913	0.8388	0.8240	0.7488	0.7061	0.6931	0.6237	0.5816	0.5660	0.5132	0.4929	0.4630	0.4421	0.5206
-0.05%	0.01%	0.05%	0.03%	0.05%	0.03%	0.01%	0.02%	0.00%	0.04%	-0.02%	0.06%	0.06%	0.06%	0.11%	0.05%	0.04%
0.7002	0.8083		0.8513	0.8243		0.7525	0.7104		0.6298	0.5856		0.5093	0.4734		0.4447	0.5070
0.7004	0.8082		0.8512	0.8242		0.7530	0.7106		0.6301	0.5857		0.5089	0.4730		0.4446	0.5064
-0.02%	0.02%		0.01%	0.01%		-0.06%	-0.03%		-0.05%	-0.02%		0.07%	0.08%		0.03%	0.13%
0.6596	0.7399	0.8011	0.7683	0.7488	0.7525	0.6891	0.6527	0.6429	0.5788	0.5390	0.5230	0.4653	0.4316	0.4257	0.4120	0.4843
0.6598	0.7396	0.8006	0.7683	0.7487	0.7527	0.6894	0.6527	0.6428	0.5786	0.5389	0.5229	0.4649	0.4316	0.4258	0.4117	0.4838
-0.03%	0.03%	0.06%	0.00%	0.02%	-0.02%	-0.04%	0.00%	0.01%	0.03%	0.03%	0.02%	0.09%	0.00%	-0.02%	0.09%	0.12%
0.6219	0.6974	0.7536	0.7229	0.7062	0.7104	0.6527	0.6192	0.6096	0.5499	0.5123	0.4961	0.4414	0.4091	0.4039	0.3921	0.4615
0.6223	0.6974	0.7535	0.7232	0.7060	0.7103	0.6527	0.6189	0.6097	0.5497	0.5119	0.4957	0.4412	0.4091	0.4038	0.3919	0.4608
-0.06%	0.00%	0.01%	-0.03%	0.03%	0.01%	0.01%	0.04%	-0.01%	0.03%	0.08%	0.08%	0.04%	0.00%	0.04%	0.04%	0.16%
0.5881	0.6804		0.7094	0.6931		0.6429	0.6096		0.5429	0.5050		0.4360	0.4027		0.3848	0.4393
0.5884	0.6802		0.7092	0.6931		0.6426	0.6094		0.5428	0.5050		0.4358	0.4022		0.3845	0.4389
-0.04%	0.03%		0.03%	0.00%		0.04%	0.04%		0.01%	0.00%		0.04%	0.14%		0.09%	0.09%
0.5451	0.6131	0.6648	0.6377	0.6240	0.6298	0.5788	0.5499	0.5429	0.4895	0.4564	0.4429	0.3937	0.3649	0.3610	0.3500	0.4115
0.5452	0.6132	0.6648	0.6375	0.6236	0.6297	0.5785	0.5494	0.5425	0.4893	0.4563	0.4427	0.3938	0.3644	0.3609	0.3500	0.4109
-0.02%	-0.01%	0.00%	0.03%	0.05%	0.00%	0.05%	0.09%	0.08%	0.03%	0.02%	0.03%	-0.03%	0.14%	0.05%	0.01%	0.14%
0.5059	0.5692	0.6170	0.5942	0.5815	0.5856	0.5390	0.5123	0.5050	0.4564	0.4258	0.4130	0.3682	0.3418	0.3372	0.3270	0.3846
0.5058	0.5693	0.6168	0.5941	0.5814	0.5856	0.5387	0.5119	0.5047	0.4561	0.4258	0.4129	0.3681	0.3416	0.3369	0.3264	0.3840
0.01%	-0.03%	0.02%	0.03%	0.03%	-0.01%	0.05%	0.06%	0.07%	0.06%	0.02%	0.01%	0.03%	0.05%	0.07%	0.18%	0.14%
0.4710	0.5475		0.5812	0.5664		0.5230	0.4961		0.4429	0.4130		0.3600	0.3347		0.3154	0.3588
0.4710	0.5475		0.5809	0.5661		0.5227	0.4960		0.4427	0.4128		0.3597	0.3346		0.3149	0.3582
-0.01%	-0.01%		0.05%	0.04%		0.05%	0.02%		0.04%	0.05%		0.08%	0.02%		0.15%	0.16%
0.4297	0.4864	0.5369	0.5404	0.5135	0.5093	0.4653	0.4414	0.4360	0.3937	0.3682	0.3600	0.3262	0.3130	0.2959	0.2816	0.3289
0.4296	0.4862	0.5368	0.5404	0.5132	0.5094	0.4649	0.4412	0.4354	0.3932	0.3676	0.3597	0.3258	0.3128	0.2959	0.2814	0.3284
0.03%	0.04%	0.03%	0.01%	0.05%	-0.03%	0.07%	0.05%	0.12%	0.11%	0.16%	0.09%	0.15%	0.05%	0.01%	0.05%	0.14%
0.3949	0.4428	0.4896		0.4932	0.4734	0.4316	0.4091	0.4027	0.3649	0.3418	0.3347	0.3130		0.2705	0.2560	0.3008
0.3947	0.4424	0.4889		0.4928	0.4733	0.4311	0.4088	0.4023	0.3647	0.3415	0.3344	0.3128		0.2703	0.2558	0.3005
0.05%	0.07%	0.13%		0.09%	0.02%	0.11%	0.06%	0.10%	0.06%	0.10%	0.08%	0.07%		0.07%	0.10%	0.09%
0.3743	0.4144	0.4404	0.4655	0.4635		0.4257	0.4039		0.3610	0.3372		0.2959	0.2705	0.2418	0.2361	0.2773
0.3740	0.4142	0.4402	0.4653	0.4631		0.4256	0.4039		0.3609	0.3369		0.2958	0.2702	0.2416	0.2355	0.2769
0.06%	0.05%	0.05%	0.04%	0.09%		0.04%	0.02%		0.04%	0.08%		0.03%	0.10%	0.09%	0.25%	0.15%
0.3908	0.4250	0.4391	0.4444	0.4423	0.4447	0.4120	0.3921	0.3848	0.3500	0.3270	0.3154	0.2816	0.2560	0.2361	0.2320	0.2663
0.3906	0.4244	0.4390	0.4440	0.4420	0.4445	0.4118	0.3917	0.3844	0.3501	0.3267	0.3151	0.2813	0.2555	0.2357	0.2315	0.2660
0.05%	0.15%	0.02%	0.09%	0.09%	0.05%	0.06%	0.09%	0.11%	-0.02%	0.11%	0.08%	0.11%	0.18%	0.19%	0.23%	0.13%
0.5022	0.5286	0.5347	0.5310	0.5208	0.5070	0.4843	0.4615	0.4393	0.4115	0.3846	0.3588	0.3289	0.3008	0.2773	0.2663	0.2871
0.5019	0.5283	0.5347	0.5307	0.5206	0.5064	0.4840	0.4612	0.4392	0.4110	0.3844	0.3583	0.3282	0.3002	0.2769	0.2659	0.2869
0.06%	0.06%	0.00%	0.05%	0.03%	0.12%	0.06%	0.07%	0.04%	0.11%	0.03%	0.12%	0.22%	0.21%	0.17%	0.15%	0.05%

Fig. 7. Comparison of Pin-by-pin Fission Rate at Outer UO_2 Fuel Assembly
(Upper: AEGIS, Middle: Monte-Carlo, Lower: (AE-MC)/MC)

3.2 Assembly Burnup Calculation

For the verification of the burnup capability, a comparison with a Monte-Carlo burnup code is carried out for PWR fuel assemblies. The continuous energy Monte-Carlo burnup code, MVP-BURN, developed by JAEA, is used in the present comparison [45]. Calculation conditions are listed in Table 2.

Comparisons of assembly k-infinities are shown in Figs. 8-10. These figures indicate that the k-infinities of the AEGIS code well reproduce the reference results of the MVP-BURN code. Since the assembly burnup calculation includes all the aspects of the lattice physics computation, the present results prove the validity of the whole calculation process of the AEGIS code.

3.3 Isotopic Composition

The accuracy of isotopic compositions is important not only for the neutronics analysis, but also for the source term analysis, as it is related to factors such as heat or gamma-ray generation. Therefore, a comparison of isotopic compositions with the MVP-BURN data is carried out for a pin-cell geometry. Calculation conditions are summarized in Table 2.

The comparison results for number densities of fission products and heavy nuclides at 30GWd/t are shown in Figs. 11-14. The maximum error for fission product nuclides is less than 1% and that for heavy nuclides is less than 2%, indicating an excellent agreement of both codes. This result is possible due to the accuracy of several elements of the AEGIS code, such as the precise resonance treatment with the ultra-fine group method and the reaction rate preservation method using the SPH factor. Since the resonance overlapping among nuclides is explicitly treated in the AEGIS code, the number densities of particular nuclides, such as ^{151}Sm, which is significantly affected by the resonance interference with ^{238}U, is accurately predicted.

3.4 Critical Experiments

As a part of integral tests of the AEGIS code, analyses of critical experiments are carried out. The critical experiments performed in LWR configurations (the B&W 1810 series critical experiments) are chosen since this series of critical experiments is well suited for verification of a lattice physics code for light water reactors [46].

Calculation conditions of the AEGIS code are summarized as follows:

Type of fuel: 2.46wt% UO_2 (Core1), 2.46wt% and 1.94wt%Gd_2O_3+4.00wt%UO_2 (Core2)

Ray separation: less than 0.2cm using the Gauss-

Table 2. Calculation Conditions for Fuel Assembly and Isotopic Composition Analyses

	Assembly calculation	Isotopic composition calculation
Type of fuel	4.1wt% UO_2, 6.1wt% Puf MOX fuel assemblies (including low, medium and high-content Pu rods), 4.1wt%UO_2 including 16 Gadolinium bearing fuel rods with 6wt%Gd_2O_3.	4.1wt% UO_2 (pin-cell geometry)
Ray separation	Less than 0.2cm using the Gauss-Legendre macroband method	Less than 0.1cm using the Gauss-Legendre macroband method
Number of azimuthal angles	48 (for 2π)	64 (for 2π)
Number of polar angles	2 (for $\pi/2$ using the TY-opt quadrature set)	
Nuclear data library	ENDF/B-VI.8 (both for AEGIS and MVP-BURN)	
Burnup calculation method	Krylov subspace method with the projected predictor-corrector (PPC) method (AEGIS), the Bateman method with the predictor corrector (PC) method (MVP-BURN)	
Temperature	HFP condition (900K, 600K and 600K for pellet, cladding and moderator, respectively)	
Boron concentration	550ppm	
Depletion	0~60GWd/t	0~30GWd/t
Depletion step	0.5GWd/t[1)]	1.0GWd/t
Number of histories of MVP-BURN (per burnup step)	4×10^6, 4×10^6, 1×10^7 for UO_2, MOX and Gd-bearing fuel assemblies, respectively.	10^6

1) 0.25GWd/t is used for MVP-BURN to reduce discretization error of coarse burnup step, since the conventional PC method is adopted in MVP-BURN.

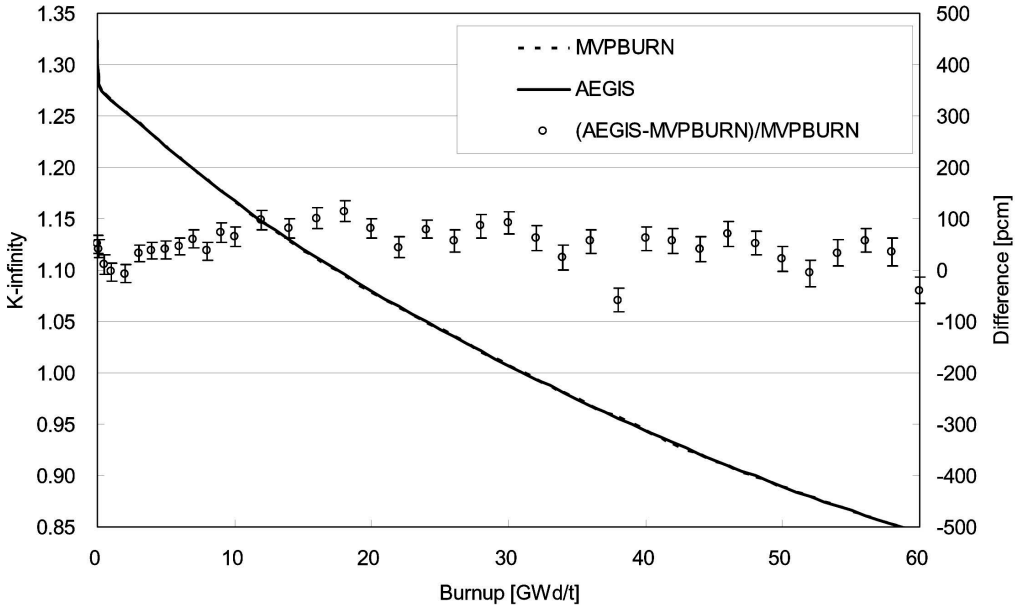

Fig. 8. Comparison of K-infinity of 4.1wt% UO_2 PWR Fuel Assembly

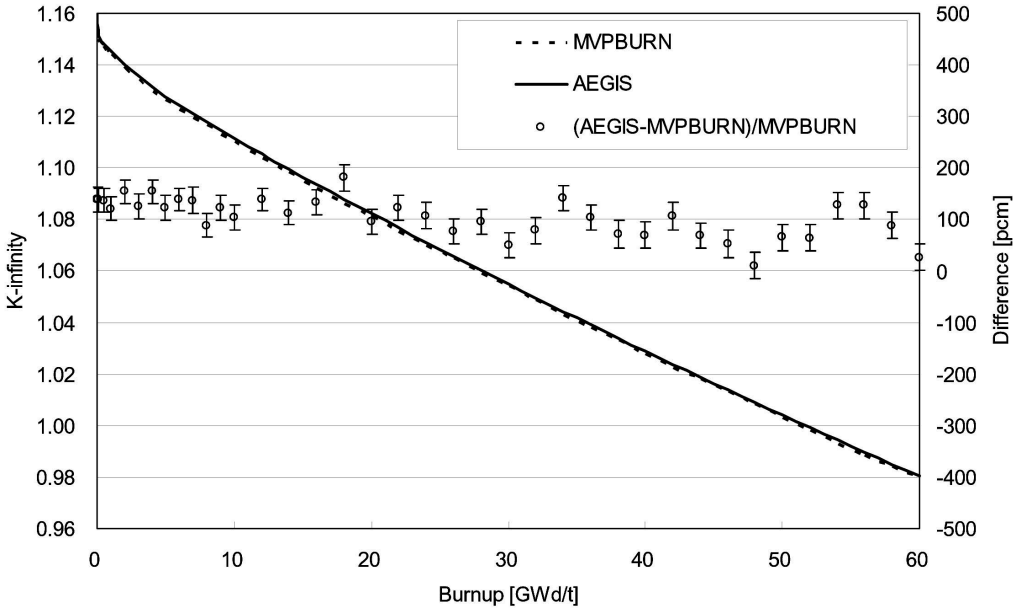

Fig. 9. Comparison of K-infinity of 6.1wt% Puf PWR Fuel Assembly

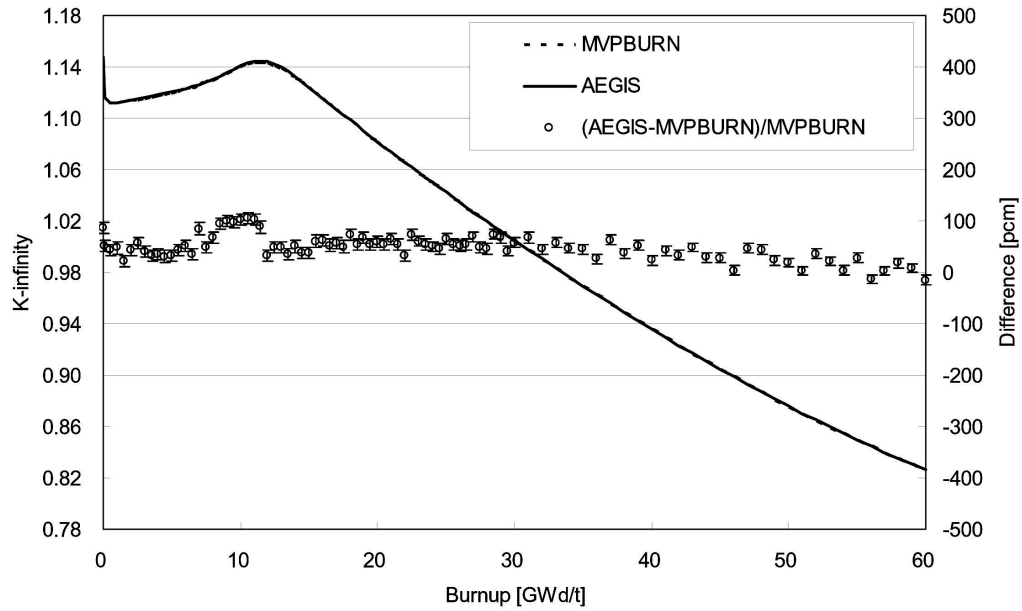

Fig. 10. Comparison of K-infinity of 4.1wt% UO_2 - 6wt%Gd_2O_3 PWR Fuel Assembly

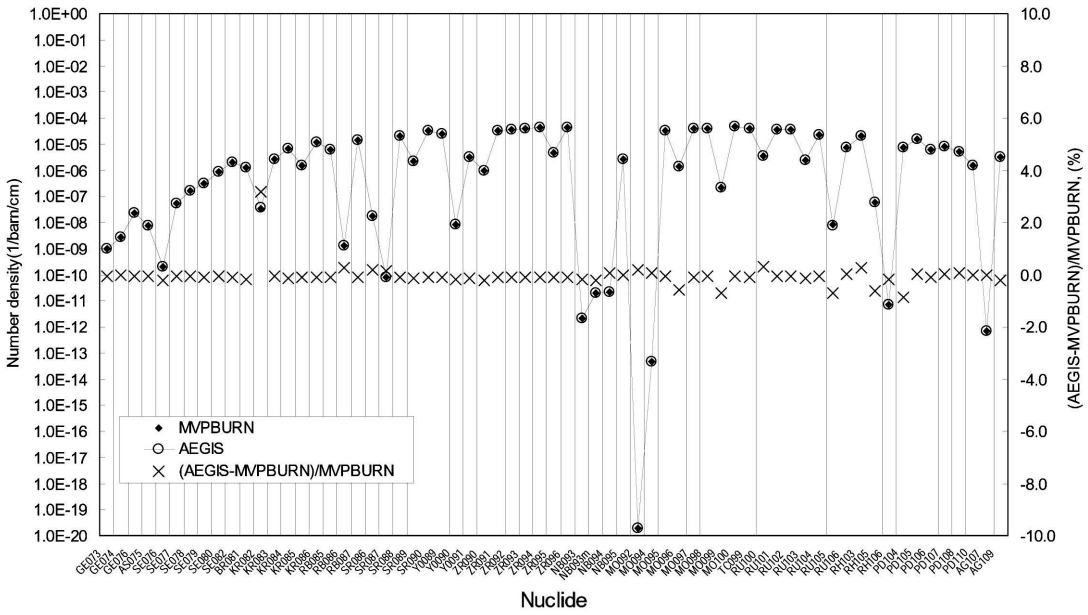

Fig. 11. Comparison of Number Density of 4.1wt% UO_2 Fuel Rod at 30GWd/t (^{73}Ge-^{109}Ag)

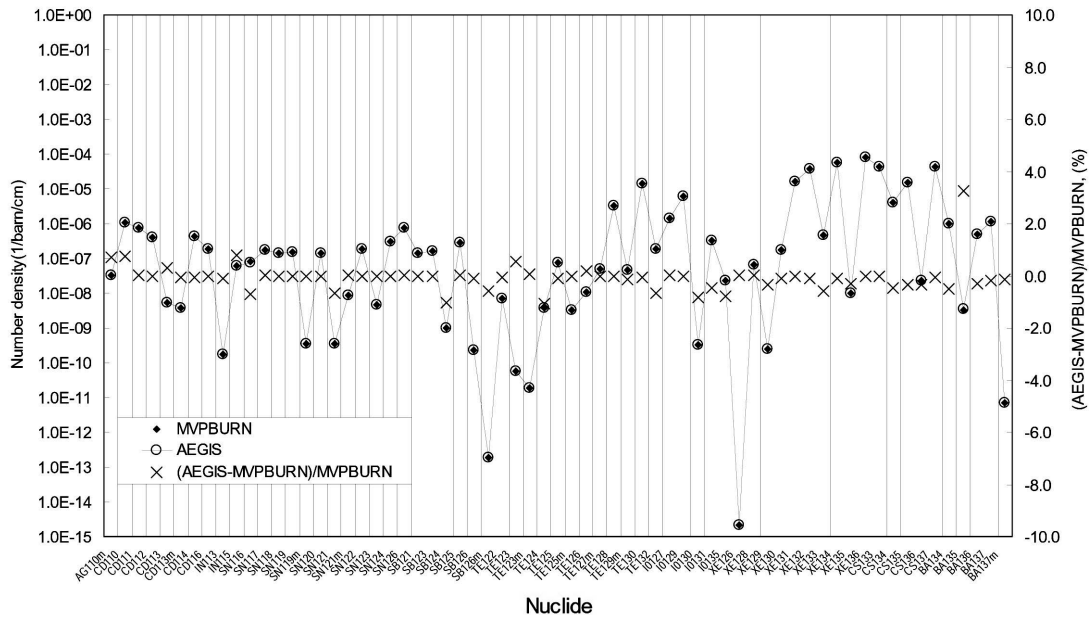

Fig. 12. Comparison of Number Density of 4.1wt% UO_2 Fuel Rod at 30GWd/t(^{110m}Ag-^{137m}Ba)

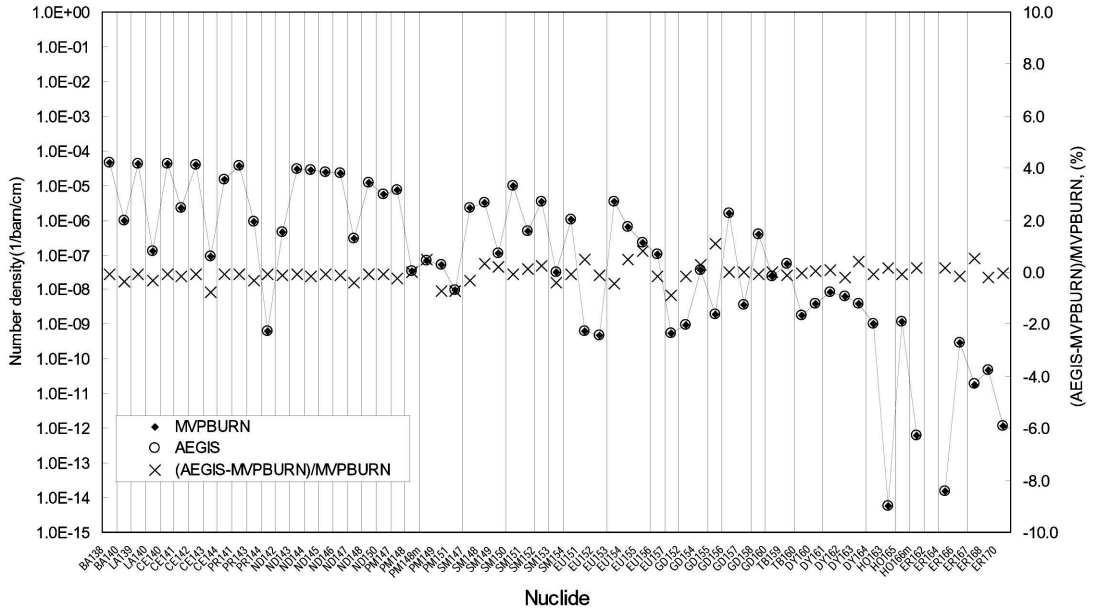

Fig. 13. Comparison of Number Density of 4.1wt% UO_2 Fuel Rod at 30GWd/t(^{138}Ba-^{170}Er)

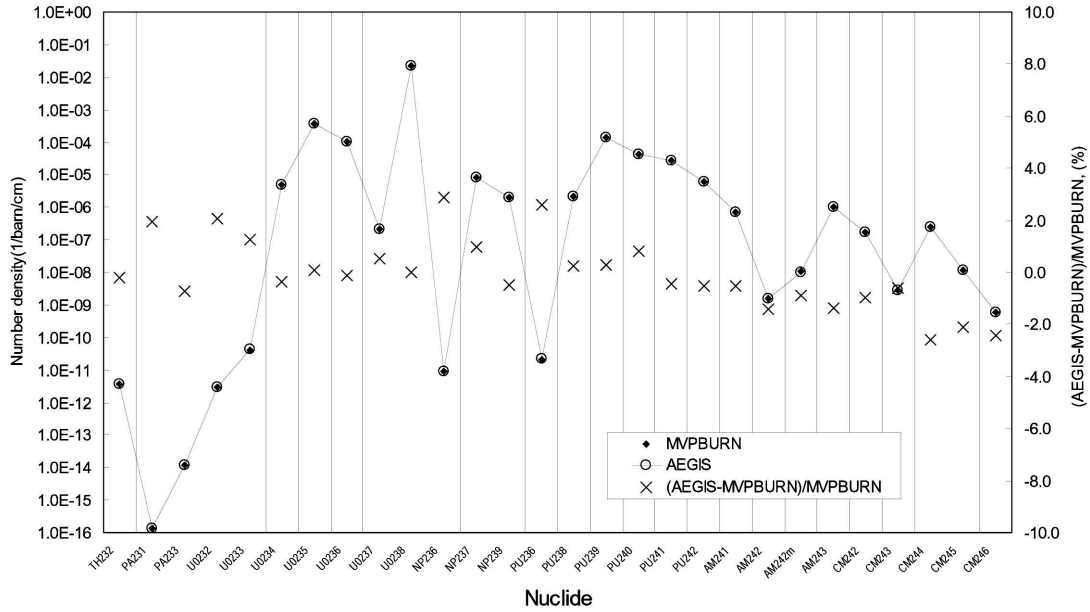

Fig. 14. Comparison of Number Density of 4.1wt% UO_2 Fuel Rod at 30GWd/t(^{232}Th-^{246}Cm)

							Measure AEGIS (A-M)/M
1.018	1.019						
1.027	1.028					RMS	0.53%
0.85%	0.85%					Max	1.18%
1.011	1.067						
1.007	1.064						
-0.38%	-0.30%						
0.987	1.012	1.081	1.054				
0.992	1.020	1.083	1.065				
0.52%	0.75%	0.21%	1.09%				
0.981	1.009	1.090	1.104				
0.988	1.016	1.084	1.103				
0.69%	0.68%	-0.52%	-0.12%				
0.997	1.058		1.086	1.059	0.988		
0.988	1.048		1.083	1.055	0.986		
-0.87%	-0.98%		-0.25%	-0.41%	-0.24%		
0.966	0.999	1.032	0.989	0.965	0.938	0.925	
0.965	0.987	1.036	0.993	0.965	0.942	0.925	
-0.15%	-1.18%	0.37%	0.37%	-0.04%	0.48%	-0.04%	
0.945	0.945	0.953	0.945	0.934	0.923	0.914	0.903
0.942	0.947	0.954	0.945	0.934	0.923	0.912	0.902
-0.27%	0.25%	0.14%	0.02%	-0.02%	-0.05%	-0.25%	-0.11%

Fig. 15. Comparison of Pin-by-pin Fission Rate Distribution at B&W Core 1 Experiment

								Measure AEGIS (A-M)/M
1.005	0.999							
1.015	1.014						RMS	0.86%
0.95%	1.48%						max	2.14%
0.913	1.017							
0.919	1.020							
0.64%	0.28%							
0.170	0.931	0.988	0.181					
0.173	0.929	0.986	0.177					
1.98%	-0.26%	-0.21%	-2.14%					
0.932	1.007	1.087	1.050					
0.936	1.011	1.080	1.047					
0.44%	0.37%	-0.63%	-0.29%					
1.036	1.125		1.131	1.048	0.187			
1.051	1.121		1.134	1.034	0.185			
1.42%	-0.37%		0.30%	-1.32%	-1.25%			
1.063	1.094	1.158	1.088	1.035	0.963	1.018		
1.076	1.100	1.153	1.094	1.031	0.960	1.014		
1.18%	0.59%	-0.41%	0.59%	-0.38%	-0.36%	-0.42%		
1.072	1.089	1.100	1.086	1.070	1.054	1.060	1.070	
1.085	1.091	1.098	1.085	1.065	1.049	1.057	1.067	
1.25%	0.15%	-0.16%	-0.13%	-0.47%	-0.46%	-0.31%	-0.25%	

Fig. 16. Comparison of Pin-by-pin Fission Rate Distribution at B&W Core 5 Experiment

Legendre macroband method

Number of azimuthal angles: 48 (for 2π)

Number of polar angles: 2 (for $\pi/2$ using the TY-opt quadrature set)

Nuclear data library: ENDF/B-VII

Note that axial leakage is considered through the buckling correction in removal cross sections. K-effectives evaluated by the AEGIS code for Cores 1 and 5 are 1.00152 and 1.00057, respectively, showing good agreement with experiments (1.00000). Comparisons of pin-by-pin fission rate distribution are shown in Figs. 15 and 16. The errors in pin-by-pin fission rates are small even for Gadolinia bearing fuel rods. These results demonstrate the validity of the AEGIS code as a whole core transport code.

4. SUMMARY

The AEGIS code is an advanced lattice physics code mainly used for LWR analyses. In the present paper, an overview of the calculation methodology and verification/validation results of the AEGIS code was presented.

In order to increase the accuracy and efficiency of a lattice physics calculation, various numerical algorithms are implemented in the AEGIS code. The validity of the AEGIS code is confirmed through the various benchmark calculations.

The AEGIS code will be used as a lattice physics code for SCOPE2, which is a three-dimensional pin-by-pin core analysis code for PWRs. The precise physics models implemented in the AEGIS code contribute to enhance the robustness and fidelity of core simulations, especially in severe situations, e.g., situations with large spectral mismatch, strong heterogeneity and considerable variation from the current operating conditions, which may appear during future reactor operations.

REFERENCES

[1] M. Tatsumi, A. Yamamoto, ‘‘Advanced PWR Core Calculation based on Multi-group Nodal-transport Method in Three-dimensional Pin-by-pin Geometry,’’ J. Nucl. Sci. Technol., 40, 376 (2003).

[2] R. E. MacFarlane. RSICC Peripheral Shielding Routine Collection : NJOY99.0, Code System for Producing Pointwise and Multigroup Neutron and Photon Cross Sections from ENDF/B Data. Oak Ridge National Laboratory. PSR-480 NJOY99.0.

[3] M. B. Chadwick et al., “ENDF/B-VII.0 Next Generation Evaluated Nuclear Data Library for Nuclear Science and Technology,” Special Issue on Evaluated Nuclear Data File ENDF/B-VII.0 Nuclear Data Sheets, 107(12), 2931–3059 (December 2006).

[4] E. Sartori, Standard Energy Group Structures Of Cross Section Libraries For Reactor Shielding, Reactor Cell and Fusion Neutronics Applications: VITAMIN-J, ECCO-33, ECCO-2000 and XMAS, JEF/DOC-315, Revision 3, NEA Data Bank, Gif-sur-Yvette Cedex, France, December 11, 1990.

[5] T. Ushio, T. Takeda, M. Mori, “Neutron Anisotropic

Scattering Effect in Heterogeneous Cell Calculations of Light Water Reactors," J. Nucl. Sci. Technol., 40, 464 (2003).
[6] N. Sugimura, A. Yamamoto, "Resonance Treatment Based on Ultra-fine-group Spectrum Calculation in the AEGIS code," J. Nucl. Sci. Technol., 44, 958 (2007).
[7] J. F. Briesmeister, Ed., MCNP™ – A General Monte Carlo N-Particle Transport Code, LA-13709-M, March, 2000, (2000).
[8] T. Mori, M. Nakagawa, MVP/GVMP: General Purpose Monte-carlo Codes for Neutron and Photon Transport Calculations based on Continuous Energy and Multigroup Methods," JAERI-DATA/Code 95-007, (1994).
[9] A. Yamamoto, K. Tada, N. Sugimura, T. Ushio, M. Mori, "Generation of Cross Section Library for Lattice Physics Code, AEGIS," Proc. Physor2006, Vancouver, Canada, Sep,10-14, 2006, (2006). [CD-ROM]
[10] A. M. Weinberg, E. P. Wigner, "The Physical Theory of Neutron Chain Reactors," The University of Chicago Press, Chicago (1958).
[11] M. Tabuchi, N. Sugimura, T. Ushio et al., "Verification of the Resonance Calculation model for Rod Cluster Control Based on Ultra-fine-group Spectrum Calculation in the AEGIS code," Proc. International Conference on Mathematics, Computational Methods & Reactor Physics (M&C 2009), Saratoga Springs, NY, May 3-7, 2009, (2009). [CD-ROM]
[12] R. J. J. Stamm'ler, M. J. Abbate, Methods of Steady-State Reactor Physics in Nuclear Design, Academic Press, London, ISBN0-12-663220-7 (1983).
[13] A. Yamamoto, N. Sugimura, T. Ushio, "Calculation Models of AEGIS, an Advanced Neutronics Solver of Next Generation," Trans. Am. Nucl. Soc., 92, 631 (2005).
[14] N. Sugimura, A. Yamamoto, "Evaluation of Dancoff Factors in Complicated Geometry using the Method of Characteristics," J. Nucl. Sci. Technol., 43, 1182 (2006).
[15] V. S. Valdimirov, Ph.D. Thesis, V.A. Stecjlova Mathematics Institute, USSR (1959).
[16] K. Takeuchi, "A Numerical Method for Solving the Neutron Transport Equation in Finite Cylindrical Geometry," J. Nucl. Sci. Technol., 6, 141 (1969).
[17] K. Takeuchi, "Numerical Solution of Space-Angle Energy Dependent Neutron Integral Transport Equation," J. Nucl. Sci. Technol., 8, 141 (1971).
[18] M. J. Halsall, CACTUS, A Characteristics Solution to the Neutron Transport Equation in Complicated Geometries, AEEW-R 1291, (1971).
[19] R. Askew, A Characteristics Formulation of the Neutron Transport Equation in Complicated Geometries, AEEW-M 1108 (1972).
[20] D. Knott, KRAM:A Lattice Physics Code for Modeling the BWR Fuel Designs, Ph.D. Thesis, Pennsylvania State University, (1990).
[21] N. Z. Cho, S. G. Hong, ''CRX: A Transport Theory Code for Cell and Assembly Calculations based on Characteristics Method,'' Proc. Int. Conf. on Physics of Reactors, PHYSOR96,Sep. 16–20, Mito, Japan, 1, A-80 (1996).
[22] H. G.. Joo, J. Y. Cho, K. S. Kim et al. "Methods and Performance of a Three-dimensional Whole-core Transport Code DeCART," Proc. PHYSOR2004, Paper 95599, April 25–29, Chicago, Illinois, USA. [CD-ROM]
[23] Z. Weiss, G. Ball, "Ray-Tracing in Complicated Geometries," Ann. Nucl. Energy, 18, 483 (1991).
[24] J. T. West, M. B. Emmet, "MARS: A multiple array system Using Combinatorial Geometry," Oak Ridge National Laboratory, Radiation Shielding Information Center Report, Dec. 1980, (1980).
[25] T. Jevremovic, J. Vujic, and K. Tsuda, "ANEMONA—A Neutron Transport Code for General Geometry Reactor Assemblies Based on the Method of Characteristics and R-Function Solid Modeler," Ann. Nucl. Energy, 28,125 (2001).
[26] E. A. Villarino et al., "HELIOS: Angularly Dependent Collision Probabilities," Nucl. Sci. Eng., 112, 16 (1992).
[27] N. Sugimura, A. Yamamoto, T. Ushio, M. Mori, M. Tabuchi, T. Endo, "Neutron Transport Models of AEGIS: An Advanced Next-Generation Neutronics Design System," Nucl. Sci. Eng., 155, 276 (2007).
[28] A. Leonard, C. T. McDaniel, ''Optimal Polar Angles and Weights,'' Trans. Am. Nucl. Soc., 73, 171 (1995).
[29] R. Sanchez, L. Mao, S. Santandrea, ''Treatment of Boundary Conditions in Trajectory-based Deterministic Transport Methods,'' Nucl. Sci. Eng., 140, 23 (2002).
[30] A. Yamamoto, M. Tabuchi, N. Sugimura, T. Ushio, M. Mori, "Derivation of Optimum Polar Angle Quadrature Set for the Method of Characteristics Based on Approximation Error for the Bickley Function," J. Nucl. Sci. Technol., 44, 129 (2007).
[31] A. Yamamoto, Y. Kitamura, T. Ushio, N. Sugimura, "Convergence Improvement of Coarse Mesh Rebalance Method for Neutron Transport Calculations," J. Nucl. Sci. Technol., 41, 781 (2004).
[32] A. Yamamoto, "Generalized Coarse-Mesh Rebalance Method for Acceleration of Neutron Transport Calculations," Nucl. Sci. Eng., 151, 274 (2005).
[33] K. D. Lathrop, F. W. Brinkley, TWOTRAN-II: An Interfaced, Exportable Version of the TWOTRAN Code for Two-Dimensional Transport, LA-4848-MS, Los Alamos Scientific Laboratory,(1973).
[34] K. S. Smith, ''Nodal Method Storage Reduction by Nonlinear Iteration,'' Trans. Am. Nucl. Soc., 44, 265 (1983).
[35] K. S. Smith, J. D. Rhodes, ''CASMO-4 Characteristics Method for Two-dimensional PWR and BWR Core Calculations,'' Trans. Am. Nucl. Soc., 83, 292 (2000).
[36] N. Z. Cho, C. J. Park, ''A Comparison of Coarse Mesh Rebalance and Coarse Mesh Finite Di_erence Accelerations for the Neutron Transport Calculations,'' Proc. Nuclear Mathematical and Computational Sciences: A Century in Review, A century A new, Gatlinburg, Tennessee, April 6–11, 2003, American Nuclear Society (2003). [CD-ROM]
[37] H.G. Joo, J. Y. Cho, H. Y. Kim et al., ''Dynamic Implementation of the Equivalence Theory in the Heterogeneous Whole Core Transport Calculation,'' Proc. Int. Conf. on the New Frontiers of Nuclear Technology: Reactor Physics, Safety and High-Performance Computing (PHYSOR2002), Oct. 7–10, 2002, 13A-02, Seoul, Korea, (2002). [CD-ROM]
[38] K. S. Smith, J. D. Rhodes III, ''Full-core, 2-D, LWR Core Calculation with CASMO-4E,'' Proc. Int. Conf. on the New Frontiers of Nuclear Technology: Reactor Physics, Safety and High-Performance Computing (PHYSOR2002), Oct. 7–10, 2002, 13A-04, Seoul, Korea, (2002). [CD-ROM]

[39] Keisuke OKUMURA, Users manual of MVP-BURN (v2.22), (2004).
[40] A. Yamamoto, M. Tatsumi, N. Sugimura, "Numerical Solution of Stiff Burnup Equation with Short Half Lived Nuclides by the Krylov Subspace Method," J. Nucl. Sci. Technol., 44, 147 (2007).
[41] A. Yamamoto, M. Tatsumi, N. Sugimura, "Projected Predictor-Corrector Method for Lattice Physics Burnup Calculations," Nucl. Sci. Eng., 163, 144 (2009).
[42] C. Moler, C. V. Loan, "Nineteen Dubious Ways to Compute the Exponential of a Matrix, Twenty-Five Years Later," SIAM review, 45, 3 (2003).
[43] M.J. Bell, ORIGEN – The ORNL Isotope Depletion and Generation Code, ORNL-4628 (1973).
[44] Benchmark on Deterministic Transport Calculations Without Spatial Homogenization, Nuclear Energy Agency, NEA/NSC/DOC(2003) 16, (2003).
[45] K. Okumura, T. Mori, M. Nakagawa, K. Kaneko, "Validation of a Continuous-Energy Monte Carlo Burn-up Code MVP-BURN and Its Application to Analysis of Post Irradiation Experiment," J. Nucl. Sci. Technol., 37, 128 (2000).
[46] L.W. Newman (Project Engineer), "Urania-gadolinia: nuclear model development and critical experiment benchmark," BAW-1810, Babcock & Wilcox, (1984).